Arabian Journal for Science and Engineering
https://doi.org/10.1007/s13369-022-06599-7

RESEARCH ARTICLE-ELECTRICAL ENGINEERING

FPGA Implementation of a Bearing Fault Classification System Based on an Envelope Analysis and Artificial Neural Network

Yassine Toumi[1] · Billel Bengherbia[1] · Sidahmed Lachenani[1] · Mohamed Ould Zmirli[1]

Received: 15 July 2021 / Accepted: 11 January 2022
© King Fahd University of Petroleum & Minerals 2022

Abstract
Bearings are one of the most widely used components of rotary machines. To keep these bearings running in the best condition, several techniques for the early diagnosis of faults are applied to enable continuous monitoring of their condition and avoid unexpected faults that may cause damage to humans and materials. Several works have focused on the development of such technologies, including those that apply artificial intelligence, in the classification and diagnosis of faults. This work reports on a multi-layer perceptron (MLP) to classify the conditions of faulty bearings, using the envelope analysis method to extract the faulty features of the bearings. The proposed architecture is implemented on a field programmable gate array (FPGA) board, where the Digilent Zybo Z7-20 platform with a Zynq-7000 FPGA circuit from Xilinx was selected as the target. The Case Western Reserve University (CWRU) dataset, which is considered the standard reference for testing bearing fault classifications, is used to evaluate the performances. The results of the implemented embedded system are first compared to those obtained through MATLAB simulations and then to those obtained from the literature. These practical results provide an average accuracy of 95 and 89% for the fault-type identification and fault-severity identification, respectively.

Keywords Bearing fault classification · FPGA · Embedded system · Envelope analysis · Multi-layer perceptron (MLP) classifier

1 Introduction

Electrical machines are utilised extensively in diverse industry applications. These machines sometimes operate under unfavourable conditions, such as high ambient temperature, high moisture and overload. These unfavourable conditions produce malfunctions in these machines that result from various faults, such as drive inverter failures, stator winding insulation breakdowns and bearing faults. Almost half of motor failures are due to the bearing [1].

Several techniques are used for diagnosing bearing faults, such as acoustic measurement, current and temperature monitoring, noise monitoring, wear debris detection, and vibration measurement [2, 3]. Amongst these techniques, the most effective is the vibration measurement because it can detect, locate and differentiate between different types of defects [4].

✉ Billel Bengherbia
bengherbia.billel@univ-medea.dz

[1] Laboratory of Advanced Electronic Systems (LSEA), University of Medea, Pole Urbain, 26000 Medea, Algeria

The diagnosis of bearing defects is based on several signal processing techniques to extract the features of the faults in the bearings. In the time domain, several characteristics, such as the peak value, root mean square, skewness, kurtosis, shape and crest factor [5, 6], are considered as the main statistical features to detect bearing defects. Although these statistical features have the advantage of simple calculations and the ability to evaluate the bearing performance, their limitations include their limited success in detecting early-stage faults, deeply distributed defects and the location of faults. In addition, many features are used to detect an easy and clear fault. In the frequency domain, the fast Fourier transform (FFT) is considered a popular and efficient tool in the spectrum analysis if the signal is under stationary conditions. The vibration signal that is obtained from the rolling bearing is often nonlinear and non-stationary [7]. As a result, FFT is inefficient at detecting these types of faults [8]. For these cases, other methods are proposed, such as envelope [9] and cepstral analyses [10, 11]. A cepstral analysis is used to detect bearing faults because it notices the periodic families in the frequency spectrum and represents them through specific peaks in the cepstrum. However, the disadvantage

Published online: 07 February 2022

of this method is that it generates many unwanted big peaks at the zero point. Once a localised defect emerges in the inner or outer race of the bearing, an impact occurs every time the rolling element crosses the defected area of the bearing race. This generates impulsive and modulating type signals, which are distinguished by the periodic repetition of sharp peaks that are modulated by high-frequency resonance components. For this reason, the envelope analysis is a well-known technique to demodulate these types of signals [12]. Moreover, numerous approaches have been suggested in the time–frequency domain, including wavelet transform (WT) [13, 14] and empirical mode decomposition (EMD) [15, 16]. The advantage of this domain is that it can handle both stationary and non-stationary vibration signals. However, this domain has several limitations. For example, the main limitation of the WT is how to select the appropriate wavelet function, which is important because of the existence of many wavelet functions that can be used to detect and diagnose bearing faults [17]. Another limitation is that this approach suffers from energy leakage. Moreover, the EMD has several weaknesses, such as end effects, sifting stop criterion and mode mixing [18, 19]. In general, although time–frequency techniques are successful when dealing with non-stationary signals, they are usually complicated, not totally independent and are complement one another in many cases.

The envelope analysis was demonstrated to be effective for the diagnosis of bearings faults. Guo et al. [20] proposed a solution based on the Hilbert transform (HT) method for extracting the envelope. In addition, they used three support vector machines (SVM) classifiers to classify the following defects: the ball, outer and inner. Tyagi and Panigrahi [21] used an envelope analysis and particle swarm optimisation (PSO) to identify the bearing faults. PSO was used to calculate the central frequency and optimal bandwidth of a bandpass filter. In [22], Amini et al. applied an envelope analysis of acoustic emission signals to detect and evaluate the damage on the bearings of freight wagons. The research by Smith and Randall in a reference study [23] used three diagnostic techniques (envelope analysis of the raw signal, cepstrum pre-whitening and a benchmark method) to classify the diagnosis outcomes of the Case Western Reserve University (CWRU) data in six categories.

In addition to the envelope analysis, machine-learning algorithms can play a key role in the classification of bearing faults, and several studies have been proposed in the literature [24] that aim to improve the classification results. Unal et al. [25] suggested a technique based on an envelope analysis accompanied by the HT, FFT and an artificial neural network (ANN) that was optimised by a genetic algorithm. Ben et al. [26] proposed using the EMD energy entropy for feature extraction and an ANN network to classify the bearing condition in seven different states (healthy, degraded inner race, degraded outer race, degraded roller, failure inner race, failure outer race and failure roller). A new approach to extracting bearing fault features was proposed by Kuncan et al. [27], which is based on a statistical method that uses patterns that are obtained by comparing the different neighbours of each of the values that appear in a one-dimensional vibratory signal. In addition, the authors use SVM, BayesNet, Random Forest, ANN network and k-nearest neighbour (KNN) to classify the ball, inner and outer bearing defects. According to Li et al. [28], three entropy approaches are used with time and frequency features to classify the bearing defects using six classifiers, including back-propagation neural network (BPNN), extreme learning machine (ELM), KNN, softmax regression (SR), logistic regression (LR) and SVM. The aim of this research study is to identify the type and severity of each defect from the vibration signals that are obtained from the CWRU dataset [29]. Laala et al. [30] proposed a method that combined wavelet package decomposition (WPD) and ANN to detect bearing faults. The WPD is used to decompose the vibration signal into a set of sub-signals, where the energy that is related to the most sensible coefficients that contain the greatest dominant fault information is selected as a distinctive feature fault. These features are used as the input of ANN to identify the bearing fault type. Sikder et al. [31] proposed a technique that involves extracting power features from the motor vibration data using power spectral density (PSD) and ELM to classify the bearing faults. They used the multitaper method (MTM) to estimate the PSD of the vibration signal and five different learning methods for the ELM, where they concluded that the "modular" learning method performs best. An approach to identify the type and level of failure that may occur in bearings and rotor bearings or in the foot of the motor in a single-phase capacitor motor was developed by Bicakci et al. [32]. This approach defined the frequency and amplitude values of the first five harmonics of the FFT of the vibration signal and two different ANNs that were customised separately and developed to determine the type and rate of the motor failure. Meserkhani et al. [33] used different parameters and features in the time domain that were extracted from the signal, and four states (one healthy and three faulty states) were identified based on these. An ANN was used to separate, detect and classify defect sizes.

Because of the complexity of the approaches that have been proposed to detect and classify bearing faults, which generally require complex and specific pre-processing to determine the signatures of the faults, their implementation in systems on a chip (SoC) represents a challenge for researchers. There are multiple challenges to achieve efficient implementations in the hardware of embedded intelligence (EI), such as the necessity for the following: (1) low power consumption; (2) high computational processing; and (3) scalability to accommodate diverse network topologies and

sizes [34]. The fast growth of ANNs has sped up the development of several implementation architectures through several platforms, such as graphics processing units (GPUs), central processing units (CPUs) and FPGA. However, large-scale deep-learning topologies require a large amount of parallel processing, memory resources, important processing power and high throughput, due to the structure and function of ANNs. In addition, in the context of real-time hardware systems, it is important to find the right trade-off between energy efficiency, performance, cost and fast development (e.g. by using fixed-point computations and appropriate quantised memory representations in place of floating-point computations). Although limited in resources and size, numerous approaches have indicated that FPGAs deliver a strong starting point for the future implementation of architectures. Consequently, implementing the solutions on an FPGA circuit is considered a promising approach, as the circuit is a specific embedded system that effectively replaces the processing of personal computers (PCs) because of its small size, portability, low cost, low power consumption and real-time applications [35, 36].

In [37], Kang et al. proposed an algorithm that makes it possible to make reliable decisions on the state of bearings. This algorithm is based on the extraction of signatures by a time–frequency analysis and the SVM. Due to the computational complexity that prevents the use of the proposed technique in real-time applications, the authors proposed an FPGA implementation of a multicore architecture that allows an online fault diagnosis. Camarena-Martinez et al. [38] offered an approach based on EMD, combined with adaptive linear element (ADALINE) neural network and feed-forward neural network (FFNN) classifier, to identify several motor faults, such as broken rotor bars, bearing defects and unbalance. The whole system is implemented on FPGA for real-time operations to analyse the characteristics of motor signals and detect the different states of the induction motor. In [39], Contreras-Hernandez et al. proposed using a quaternion signal analysis (QSA) to characterise the behaviour of temporal signals (accelerometer and current) while using a reduced number of samples. The decision tree algorithm is used to classify several types of faults, including bearing faults, which then must be implemented on an FPGA-type platform to validate its effectiveness under real operating conditions. Cabal-Yepez et al. used information entropy merged with ANN to detect the faults that occur in induction motors. The authors proposed the FPGA-based implementation of the neural networks for the automatic diagnosis of faults using the analysis of vibrational signals from a three-axis accelerometer [40]. In [41], Bengherbia et al. developed an FPGA-based wireless sensor node for a machine vibration monitoring system and fault diagnosis. The suggested wireless node is based on a Xilinx Artix7-XC7A35T circuit and connected via a serial peripheral interface to the nRF24L01 + transceiver as a low-power and low-cost wireless radio module. In continuous work [42], the authors replaced the FFT processing of vibrational signals with an ADALINE neural network to extract the harmonics and identify the faults in rotating machines.

In this work, we designed and implemented an embedded intelligent system to diagnose bearing faults. The system includes a bearing state signature extraction through envelope analysis and reliable decision-making using a multilayer perceptron (MLP), which significantly decrease the FPGA's hardware resource utilisation while maintaining acceptable accuracy. In this context, we implement the proposed architecture on the Digilent Zybo Z7-20 platform with a low-cost and low-energy consumption FPGA circuit from Xilinx. This approach provides an intelligent system that has been tested with the CWRU bearing data, following the recommendations by the two benchmark studies [23, 28], where they conclude that some combinations of data from this dataset make it easy to classify the fault types or fault severities, while several combinations are difficult for pattern identification. In addition, most existing fault diagnosis research works using this dataset have several limitations, such as the absence of a comprehensive analysis of bearing fault variations and diversity and only focusing on certain bearing fault combinations. This led to the saturation of the classification accuracy (almost 100%).

The proposed method initially extracts the envelope of the raw signal through the HT, and the envelope spectrum is calculated by applying FFT. This makes it possible to determine the amplitude of the frequency peaks, which characterise the fault type. The determined peak's amplitudes are used as input features for the MLP classifier. The computational complexity in the suggested system limits its use in real-time applications. To address this issue, we propose an FPGA implementation that provides a high processing capacity and a low computation time by exploiting the hardware/software co-design approach. This amounts to optimally embedding a processor in the FPGA and custom IP-cores for the envelope analysis and MLP network. A program that is written in C is executed to manage the various tasks in the system. The aims are to keep the flexibility of the processor while taking advantage of the hardware resources that are available in the FPGA to improve the real-time performance.

The remainder of the paper is organised as follows: Sect. 2 focuses on the theories regarding the bearing fault characteristic frequencies, envelope analysis and MLP; Sect. 3 presents the architectural design of the proposed algorithms; Sect. 4 describes the CWRU dataset; Sect. 5 presents the experimental tests and results; and Sect. 6 provides the conclusion.

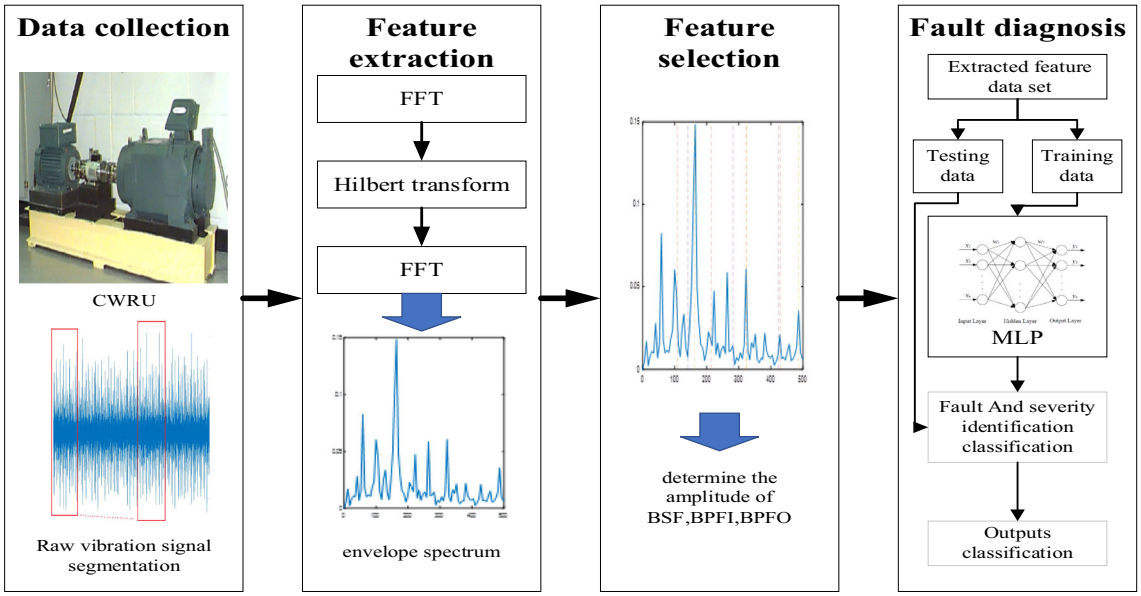


Fig. 1 Flowchart of the proposed fault diagnosis method

2 Proposed Method

This section presents the proposed method. Figure 1 illustrates the flowchart for the suggested method. First, the raw vibration signal of the bearing is segmented into sub-signals. Second, the envelope spectrum is calculated. Third, the amplitudes corresponding to the bearing fault frequency characteristics are determined. Finally, the MLP classifier is used to diagnose the bearing fault type and its severity fault. The principle of each step is discussed in detail in the following sections.

2.1 Bearing Fault Frequencies

Most rolling bearings consist of an inner and outer ring. Between these two rings, the rolling elements are kept at an equal distance from each other by a cage that guides them and facilitates their rotation, thus preventing contact between them. The standard shapes of the rolling elements include the following two categories: balls and rollers. The rollers are classified according to their forms and we distinguish between the symmetrical and asymmetrical cylindrical, taper and needle rollers. Because bearings are composed of multiple parts, they are the most fragile components in rotating machinery, where a characteristic fault frequency is associated with each of the four parts that make up the bearing. Defects that appear on the bearings are manifested by the appearance of periodic shocks at certain frequencies. To achieve a reliable diagnosis from the spectrum of the vibration signal, we can use a certain number of characteristic frequencies. These frequencies are noted as follows:

- **Ball pass frequency inner** (**BPFI**) or inner race failure frequency. We assume a given point of the inner track, and this frequency corresponds to the number of balls (or rollers) that pass through this point each time the shaft makes a complete rotation.
- **Ball pass frequency outer** (**BPFO**) or outer race failure frequency. We assume a given point of the outer track, and this frequency corresponds to the number of balls (or rollers) that pass through this point each time the shaft makes a complete rotation.
- **Ball spin frequency** (**BSF**) or rolling element failure frequency. This corresponds to the number of turns that a bearing ball (or roller) makes each time the shaft makes a complete rotation.
- **Fundamental train frequency** (**FTF**) or cage failure frequency. This corresponds to the number of turns that the bearing cage makes each time the shaft makes a complete rotation.

The different frequencies depend on the rotation speed, and the geometric dimension can be calculated using the following equations:

$$\mathrm{BPFI} = \frac{\mathrm{nf_r}}{2}\left(1 + \frac{d}{D}\cos\alpha\right) \tag{1}$$

$$\mathrm{BPFO} = \frac{\mathrm{nf_r}}{2}\left(1 - \frac{d}{D}\cos\alpha\right) \tag{2}$$

$$\mathrm{BSF} = \frac{\mathrm{Df_r}}{2d}\left(1 - \left(\frac{d}{D}\cos\alpha\right)^2\right) \tag{3}$$

$$\mathrm{FTF} = \frac{f_\mathrm{r}}{2}\left(1 - \frac{d}{D}\cos\alpha\right) \tag{4}$$

where n is a number of ball (rolling) elements, f_r is the shaft speed, d is the ball bearing diameter, D is the pitch bearing diameter and α is the bearing contact angle.

2.2 Envelope Analysis

The envelope analysis is an efficient method of extracting the fault features from impulsive and modulating signals and can be found in many electrical machinery components, such as a bearing [21]. This type of signal has an amplitude modulation (AM) effect on the characteristic frequencies of the bearing.

The following three steps illustrate the envelope analysis methodology: bandpass filtering, envelope extraction and envelope spectrum calculation. The bandpass filter is used to eliminate random noises outside the bandpass, in addition to the low frequency, high amplitude signals that are created by unbalancing or misalignment, which allows one to obtain a good signal-to-noise-ratio (SNR) [43]. The envelope extraction step is performed via the HT, as its implementation in the frequency domain is the most efficient method for this step [44]. In this case, the analytic signal of the input x is processed using Eqs. (5)–(7) as follows:

$$Z_\mathrm{in} = \mathrm{fft}(x) \tag{5}$$

$$Z_\mathrm{a}(n) = \begin{cases} Z_\mathrm{in}(n) & , \quad if n = 0, \dfrac{N}{2} \\ 2Z_\mathrm{in}(n) & , \quad if 0 < n < \dfrac{N}{2} \\ 0 & , \quad if \dfrac{N}{2} < n < N \end{cases} \tag{6}$$

$$z_\mathrm{a} = \mathrm{ifft}(Z_\mathrm{a}) \tag{7}$$

where Z_in is the Fast Fourier Transfer of x, z_a is the Invers Fast Fourier Transfer of Z_a, and n is the index of data sequence with the length of N [45].

At the end, a complex signal is created, where the real part is the original signal and the imaginary part is the HT of the original signal. The envelope of the signal can be calculated using Eq. (8).

$$z_\mathrm{env} = \sqrt{z_\mathrm{a} \times \mathrm{conj}(z_\mathrm{a})} \tag{8}$$

Finally, the spectrum of the envelope can be computed by Eq. (9).

$$Z_\mathrm{env} = |\mathrm{fft}(z_\mathrm{env})| \tag{9}$$

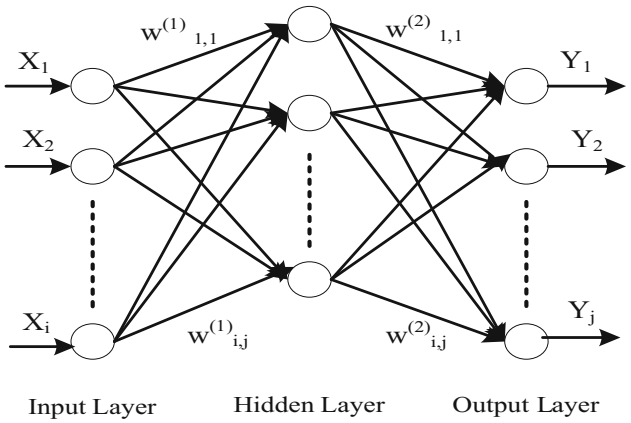


Fig. 2 Structure of the MLP

2.3 MLP

ANNs considered an important classification method in the field of machine monitoring. Their use in industrial supervision applications has proven to be effective in the early detection of machine failures and avoids unpredictable breakdowns in the production chain. Several architectures for ANN have been proposed, and the most usable one for the classification of machine faults is the MLP architecture [40].

MLP networks are composed of the following three essential layers: input, output and one or more hidden layers. Each layer is composed of a certain number of neurons. The structure is illustrated in Fig. 2. In MLP networks, each product of the input elements (x_i) and weights (w_i) is fed to summing junctions and summed with the neuron bias (b). The resulting sum passes through an activate function (f), which generates an output (y) that is like that shown in Eq. (10). Although there are several activation functions, the most common ones are as follows: hyperbolic tangent (Eq. 11), logistic sigmoid (Eq. 12), and linear functions (Eq. 13).

$$y = f\left(\sum_{i=1}^{I} w_i x_i + b\right) \tag{10}$$

$$f(n) = \frac{1 - e^{-2n}}{1 + e^{-2n}} \tag{11}$$

$$f(n) = \frac{1}{1 + e^{-n}} \tag{12}$$

$$f(n) = n \tag{13}$$

The MLP is trained by the back-propagation (BP) algorithm, which follows a learning procedure based on iterative adjustments of the weights and biases to minimise the error between the actual and predicted values (target values) of the ANN model. The training process continues until the error decreases to an acceptable value. The error function that is

applied for this purpose is usually the mean square error (MSE), which is presented in Eq. (14).

$$e = \frac{1}{2}\sum_{k=1}^{Q}(t(k) - y(k))^2 \tag{14}$$

where t is the target, y is MLP output, Q is the sample size and k is the sample number [25].

Finally, the updated weights are provided by the Eq. (15) as follows:

$$w_{i,j}(k+1) = w_{i,j}(k) - \left[\eta\frac{\partial e}{\partial w_{i,j}} + \beta\Delta w_{i,j}(k-1)\right] \tag{15}$$

where η is the learning rate and β is the momentum term, β is used to increase the speed of convergence.

3 Design, Implementation and Test of the Proposed Diagnosis System

To meet the requirements of a monitoring system for the fault diagnosis in rotating machines in terms of rapidity and reliability, we have chosen an FPGA platform. This helps us to achieve our objectives due to its hardware architecture that offers a high performance in digital signal processing.

We selected a hybrid architecture, the ZynQ from Xilinx. This circuit category offers mixed architecture, which consists of two main sections. The first is a processing system section (PS), which includes an ARM Cortex A9 dual-core processor, and the second is a programmable logic section (PL), which includes configurable hardware resources. In this work, we have used the Digilent Zybo-Z7-20 platform to implement the complete proposed system. As we have chosen the hardware/software co-design technique, the functions to be accelerated, such as the envelope analysis and MLP classifier, are implemented in hardware in the logical section of the FPGA, while the other tasks in the proposed architecture are implemented in the software and will be executed by the ARM processor.

3.1 Envelope Analysis Design

As the envelope analysis is based on FFT/inverse FFT (IFFT) processing, we have chosen to use the FFT block that is available as the custom intellectual property (IP) core in the Xilinx Vivado software library. This block offers several possible configurations. Amongst them, the pipeline-streaming configuration allows continuous data processing and is suitable for real-time processing. To ensure such a configuration and guarantee a fast data transfer, a DMA IP-core has been used. Another advantage is that the same block is used for FFT and IFFT processing. To switch between the two functions, a software configuration has been designed and executed by the ARM processor. In addition, we have chosen to configure the block for 8192 points coded in a 32-bit fixed point.

Table 1 Resources consumption of the MLP IP-core

Available resources	Consumed resources	
	Fixed point	Floating point
LUTs (53,200)	16,260	26,496
DSPs (220)	68	112
Registers	2200	3232

3.2 MLP Design

As part of this work, the design of the MLP block is carried out using Xilinx System Generator (XSG) software. This fast development tool from Xilinx is integrated into the MATLAB-Simulink environment to allow the user to create highly parallel systems for FPGA. Figure 3 illustrates the proposed architecture, which comprises a single input layer, in which its inputs are the peak's amplitudes at the BPFI, BPFO and BSF frequencies. In addition, the structure includes one hidden layer that is composed of four neurons and an output layer that provides four outputs that correspond to the condition of the bearing (normal, ball fault, inner race fault and outer race fault), where this output layer is one-hot encoding. Figure 4 shows that each neuron is composed of sets of addition and multiplication blocks and memory units to store the weights and biases that were previously obtained by MATLAB offline training. The best performances are obtained using a hyperbolic tangent function for the hidden neurons and a linear function for the output neurons. Figure 5 shows the proposed architecture of the hyperbolic tangent function.

To ensure maximum accuracy, a floating-point configuration is chosen in the settings of the different blocks of the proposed MLP (Table 1). Although this choice implies a huge consumption in terms of resources (almost double compared to a fixed-point configuration), it remains an important choice to reduce diagnostic errors.

The designed MLP is first tested with simulation via MATLAB and then retested by co-simulation using the Zynq platform as a target. These tests are performed to verify the performance of the hardware block for operation at a high processing frequency and reduced time processing (low latency). At the end of this phase, we obtain a fully operational IP-core, which will be added to the overall architecture of the complete proposed embedded diagnosis system.

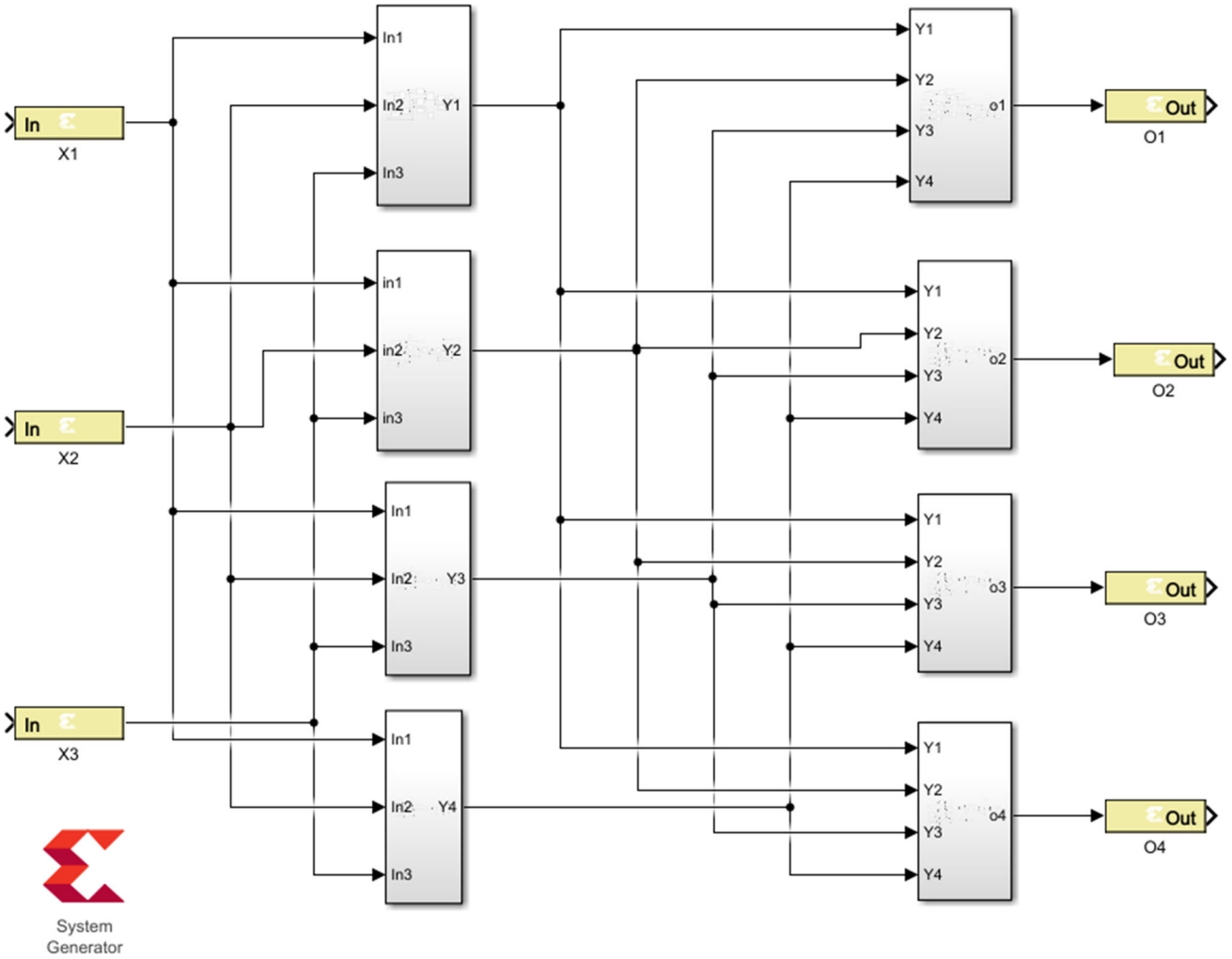


Fig. 3 Architecture of the proposed MLP using Xilinx System Generator

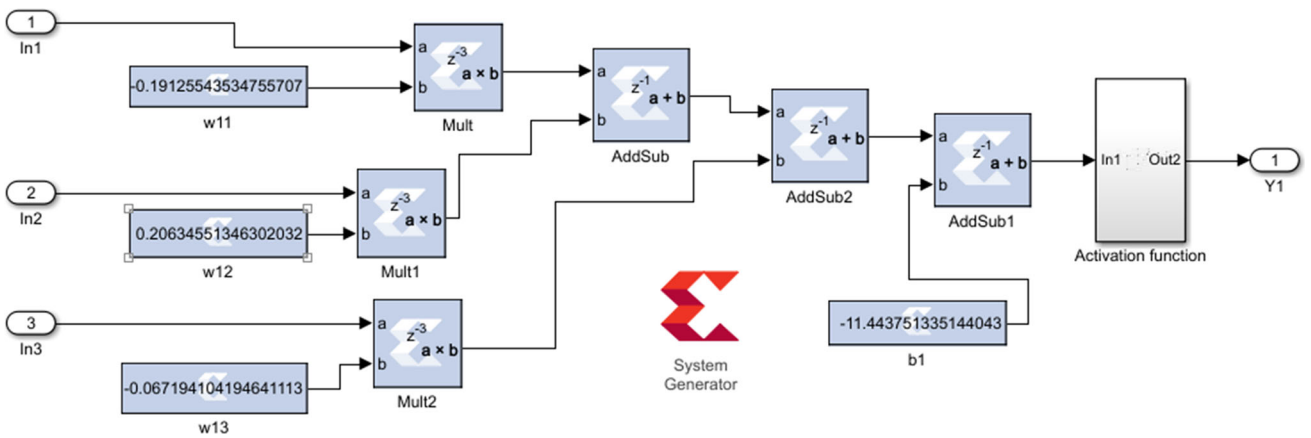


Fig. 4 Architecture of a single neuron model

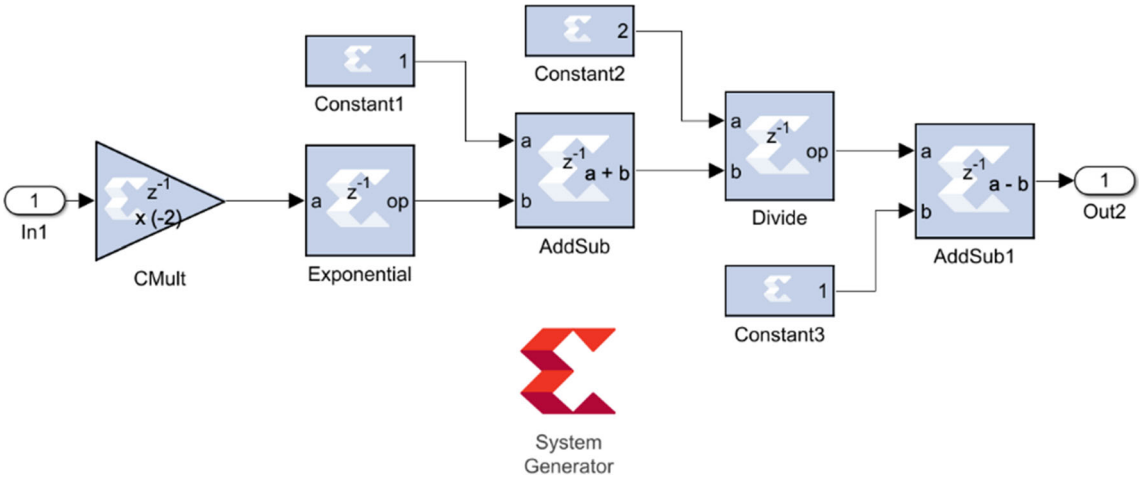


Fig. 5 Architecture of the hyperbolic

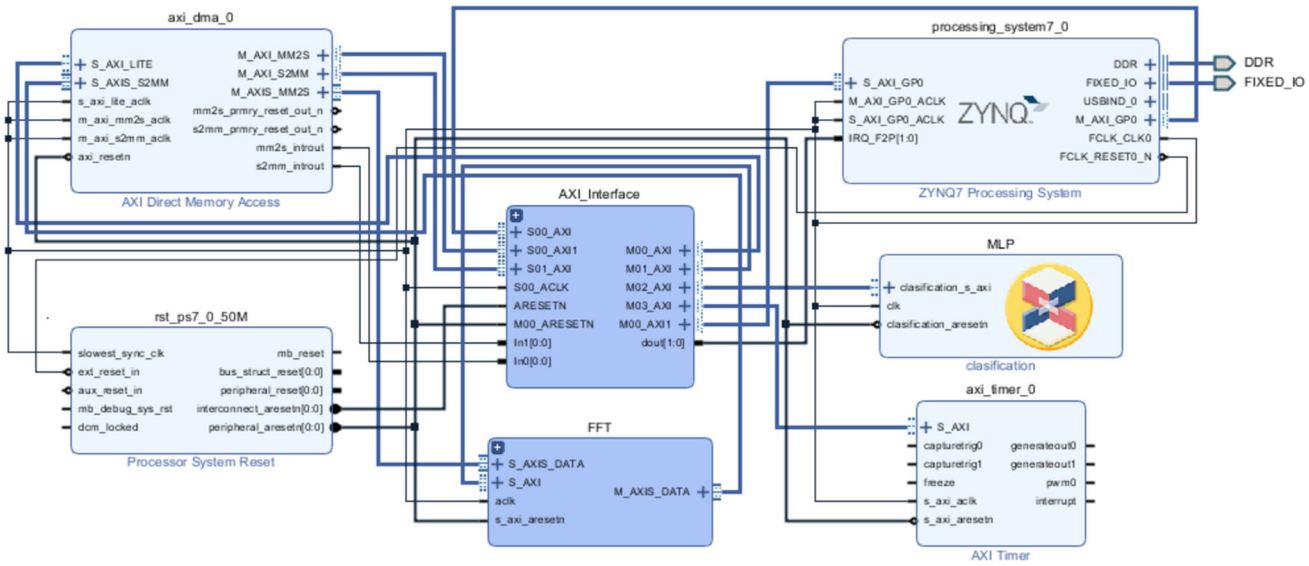


Fig. 6 Hardware Block diagram of the proposed system

3.3 Test and Results of the Complete Proposed System

The hardware system is designed with Xilinx's Vivado 2018.2. The different blocks that constitute the architecture are added in the form of IP-cores in the PL section, either from the library of the IP-cores of Xilinx, such as for the FFT block, or built beforehand and added in the architecture, such as for the MLP (Fig. 6).

The Zynq processing system that is integrated into the FPGA is used as a kernel that manages all the blocks by executing the software. These blocks in the PL section can be controlled and monitored using memory-mapped registers, which can be accessed by processors via the AXI-bus. The code is implemented using the software development kit (SDK) of Xilinx in the C language.

Table 2 FPGA resources consumption

Resource	Used/available	Utilisation (%)
LUT	34,875/53,200	65.55
LTURAM	1877/17,400	10.79
FF	17,822/106,400	16.75
BRAM	37/140	26.43
DSP	209/220	95
BUFG	1/32	3.13

The implementation results are summarised in Table 2. The results show that the resource requirement is approximately 95% of digital signal processing (DSP) slices and

65.55% of LookUp Tables (LUTs). This is due to using several multiplication blocks in the MLP architecture and the system configuration in the floating point.

To evaluate the overall performance of the FPGA implementation for the envelope analysis, the implemented full system of 8192 points of CWRU data is processed. A similar processing is also executed on the PC using MATLAB, and the results that are obtained at each step are compared with those that are obtained using the FPGA. First, the original temporal signal is processed in FFT to obtain the spectral representation of the signal, followed by an IFFT process that is carried out on the one-sided spectrum of the signal to take advantage of the symmetry in the spectrum of the original signal. Finally, the signal from the second step is processed in FFT to obtain the envelope spectrum, which characterises the fault. Figures 7, 8 and 9 illustrate the results. As shown, the signals that are obtained by the FPGA processing are like those of MATLAB.

4 Dataset Description

The vibration signals that are used in this study come from the CWRU Data Centre. This dataset has been considered in several works as a benchmark for testing and evaluating the effectiveness of new proposed techniques for diagnosing bearing defects and comparing them to existing ones. The used test bench is shown in Fig. 10 and has a 2 hp motor that reaches a maximal rotational speed of 1797 rpm on its left side. A dynamometer is placed in the right side, and a

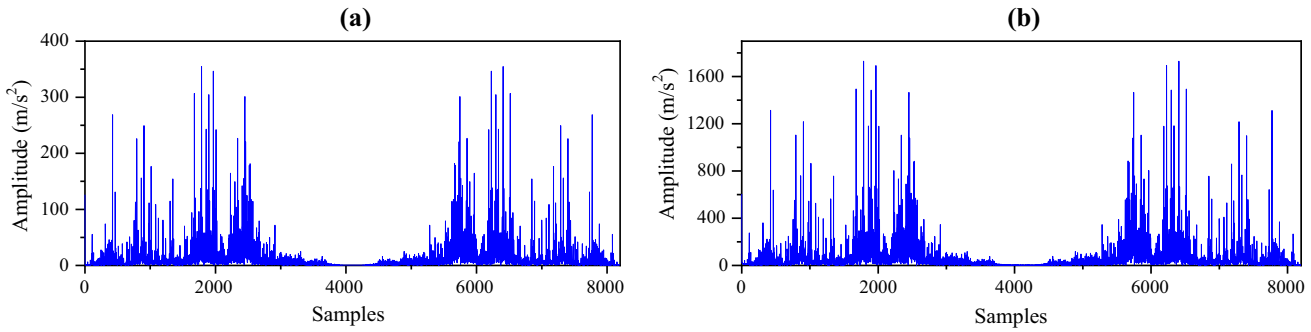


Fig. 7 FFT of the raw signal calculated by: **a** MATLAB, **b** FPGA

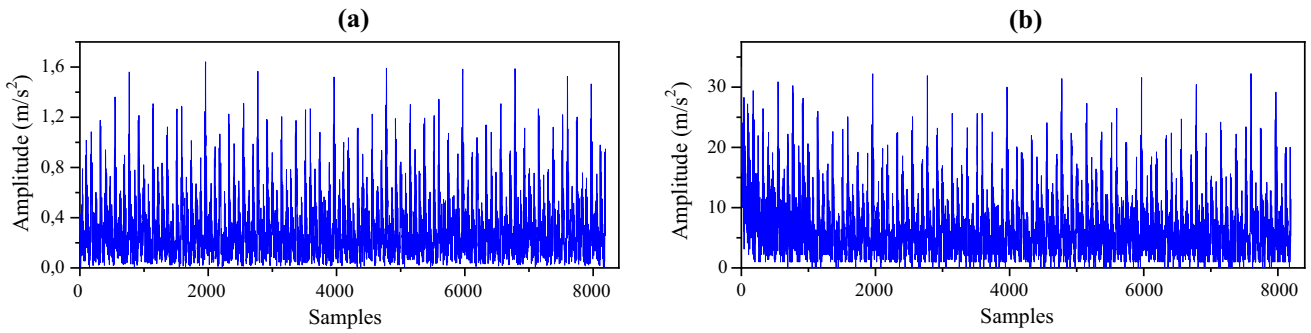


Fig. 8 IFFT processing by: **a** MATLAB, **b** FPGA

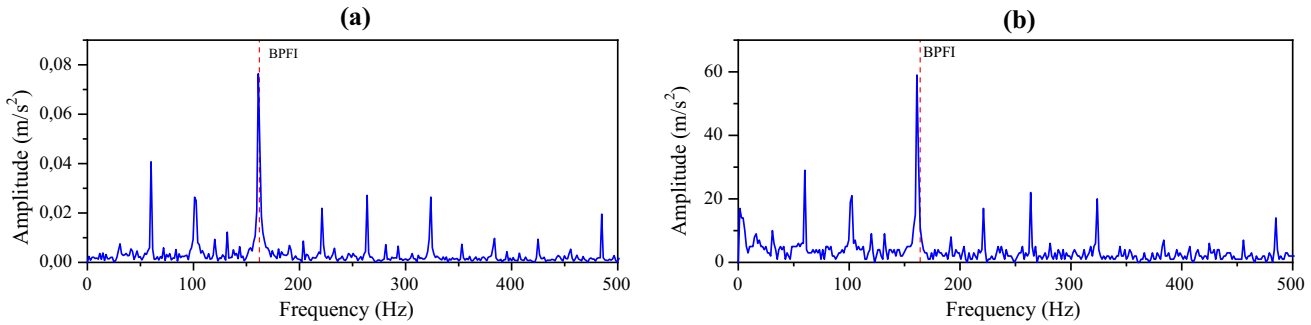


Fig. 9 Envelope spectrum by: **a** MATLAB, **b** FPGA

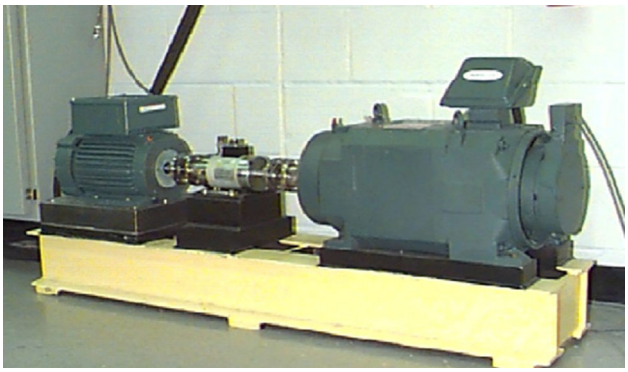


Fig. 10 CWRU bearing test rig [29]

torque transducer/encoder is placed between them. To support the motor shaft, test bearings were used with parameters, as shown in Table 3. During the experiments, single-point defects were caused in the test bearings by electro-discharge machining. To collect the vibration data, two sensors were fixed vertically to the drive end (DE) of the motor housing and the fan end (FE) of the bearing housing. The third was attached to the engine baseplate (BP) [29].

The data are recorded in sequences of more than 121,200 and 484,483 points for sampling rates of 12 and 48 kHz, respectively. The test bench collects vibration data for the following three types of faults: inner race, outer race and in the ball. The frequencies are shown in Table 4.

In this work, we are interested in identifying the type of defect and its severity. In both cases, the data obtained from measurements that were made on the bearings on the DE (12 and 48 kHz) and FE. Regarding the outer race defect, we adopted the tests that were conducted in the load area, where the sensor was positioned in the centre (6 o'clock) for the DE data and orthogonal (3 o'clock) in the load zone for the FE data.

First, each dataset's signals are segmented on data samples of 2048 and 8192 points for the sampling rate of 12 and 48 kHz, respectively, which results in a set of almost 60 data samples for each fault signal. From these 60 samples, 40 are randomly selected and divided into two groups. One group of 20 samples is reserved for training, and the second one is selected for testing. This segmentation method is like that proposed by Li et al. [28], which enables us to compare our work with theirs. In addition, we have adopted the following four fault-type identification labels: '1' (normal); '2' (ball fault); '3' (Inner race fault) and '4' (outer rate fault). For the fault-severity identification five labels, we used the following: '1' (normal); '2' (0.007 in fault); '3' (0.014 in fault); '4' (0.021 in fault) and '5' (0.028 in fault).

Regarding the DE data, for the outer race defect with a 0.028 in defect diameter, data were not collected, which limits the fault-type identification to the following three labels: normal, ball defect, inner defect. The fault-severity identification was limited to the following four labels: normal, 0.007 in, 0.014 in and 0.021 in. Regarding the FE data, for the outer race defect with a 0.021 in defect diameter and load of zero, data were not collected, which makes it possible to distinguish the following three possible cases in the fault-type identification: normal, ball defect, inner defect. Similarly, the following three cases were distinguished in the fault-severity identification: normal, a fault of 0.007 in and 0.014 in. Regarding DE data with a 48 kHz sampling rate and load of zero, only 14 data samples were selected for each fault due to the short recording of the signals, which provided 56 data samples in total. This set is reduced to only 42 in the case of 0.014 in defect diameter, because the inner race defect data were not collected. Finally, regarding the FE and DE data (48 kHz), the fault-type identification does not include the case of 0.028 in fault width because no signal was collected.

5 Experimental Results

We performed the following two categories of experimental tests (Fig. 11): fault-type identification and fault-severity identification. In addition, the results that were obtained using the FPGA board were validated by those that were simulated on a PC using MATLAB.

In the following subsections, to clarify the value of the BPFO, a red dash line is established; for the BSF, a green dash line is established; and for the BPFI a magenta dash line is established.

5.1 Fault-type Identification

Table 5 shows the classification accuracy results for each load, the different bearing defect diameters (0.007 in, 0.014 in, 0.021 in and 0.028 in) and the three datasets.

Table 3 Bearings size (in) [29]

Bearing model number	Inside diameter	Outside diameter	Ball diameter	Pitch diameter
6205-2RS JEM SKF (DE)	0.9843	2.0472	0.3126	1.537
6203-2RS JEM SKF (FE)	0.6693	1.5748	0.2656	1.122

Table 4 Defect frequencies (multiple of shaft speed in Hz) [29]

Position on rig	BPFI	BPFO	FTF	BSF
Drive end (DE)	5.4152	3.5848	0.39828	4.7135
Fan end (FE)	4.9469	3.0530	0.3817	3.9874

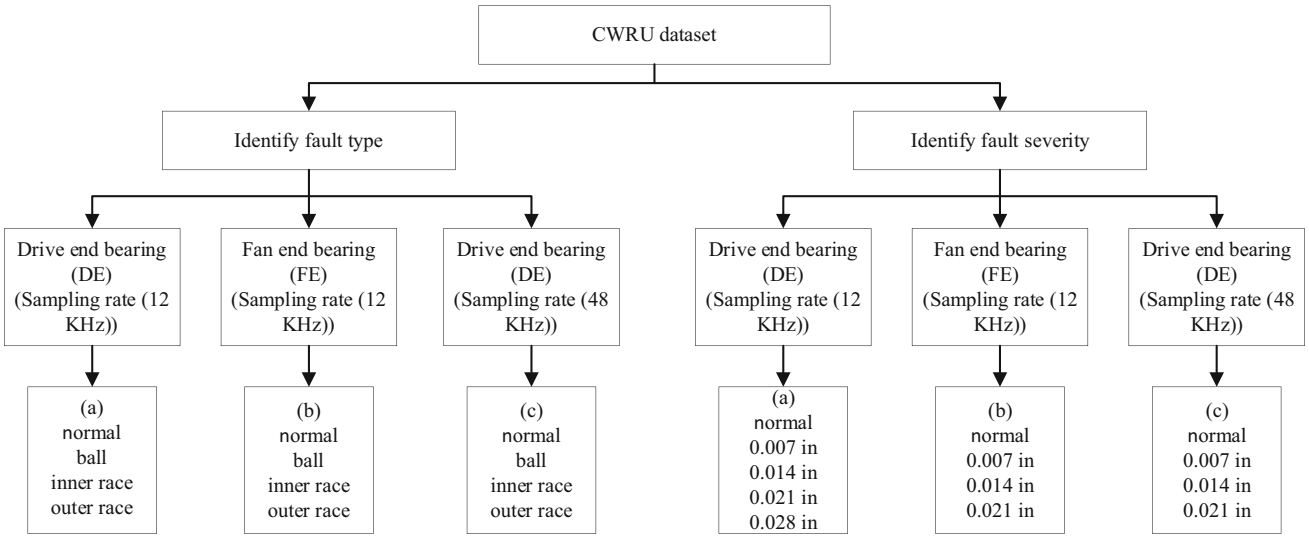


Fig. 11 Tests process flowchart

Table 5 Result of classification accuracy of fault-type identification

Fault width (in)	Load (hp)	DE (12 kHz) dataset		FE (12 kHz) dataset		DE (48 kHz) dataset	
		Using MATLAB	Using FPGA	Using MATLAB	Using FPGA	Using MATLAB	Using FPGA
0.007	0	100	100	86.25	72.5	100	100
	1	100	100	85	76.25	98.75	100
	2	100	100	86.25	72.5	100	98.75
	3	100	98.75	78.75	76.25	98.75	100
	Mean	**100**	**99.69**	**84.06**	**74.37**	**99.37**	**99.69**
0.014	0	85	78.75	98.75	100	88.10	80.95
	1	98.75	93.75	100	98.75	87.5	83.75
	2	95	91.25	100	100	83.75	82.5
	3	96.25	87.5	100	98.75	86.25	82.5
	Mean	**93.75**	**87.81**	**99.69**	**99.37**	**86.40**	**82.42**
0.021	0	100	96.25	100	80	100	87.5
	1	100	100	93.75	91.25	100	97.5
	2	100	100	92.5	91.25	100	97.5
	3	100	91.25	95	90	100	92.5
	Mean	**100**	**96.87**	**95.31**	**88.12**	100	**93.75**
0.028	0	100	95				
	1	100	95				
	2	100	93.33				
	3	100	96.67				
	Mean	**100**	**95**				

(a) DE bearing (12 kHz) dataset case
The obtained results show that the MLP classifier can easily classify the type of defect, with a test accuracy exceeding 95% in most cases. However, we recorded a minimum accuracy of 78.75% for the bearing with a defect of 0.014 in and a load of zero using FPGA. It should be noted that this result is slightly less than that obtained with MATLAB (85%). In this case, the results are shown in Fig. 12. Although the number of misclassified samples in the case of a ball fault is very large, it is not the case for the inner and outer race faults. By representing the envelope spectrum (Fig. 13) of such a situation, we can see that it is difficult to detect the peak's amplitude that corresponds to the BSF and BPFO frequencies (Fig. 13a, b, e), which justifies the difficulty that was encountered regarding the classification.

(b) FE bearing dataset case
We can observe that the defects of 0.014 in and 0.021 in could easily be identified with a test accuracy that exceeds 80%. In addition, the testing accuracy for the 0.007 in fault type decreased, with a lower test accuracy of 72.5%, which is recorded in loads zero and two using the FPGA.
To explain this, we have analysed the least accurate result for both implementations (FPGA and MATLAB). Figure 14 shows the classification results using FPGA for load two and MATLAB for load three. We note that several samples are misclassified in the case of the ball and outer faults. To explain this, Fig. 15a, b shows that the peak's amplitude at the BSF for the type of ball defect is unclear, and Fig. 15e, f shows that the peak's amplitude at the BPFO for the type of outer defect is also unclear. Therefore, we cannot identify the ball and outer defects. However, concerning the inner defect, Fig. 15c, d shows that the peak amplitude at the BPFI is clear.

(c) DE (48 kHz) dataset case
These results are in accordance with those found for the 12 kHz sampling frequency and show that the defect of 0.007 in and 0.021 in can easily be classified. However, for the bearing with a defect of 0.014 in, a minimum accuracy of 80.95% is recorded with load zero using FPGA. Figure 16 shows that some samples are misclassified in the case of the ball defect. To explain this phenomenon, Fig. 17 shows the envelope spectrum representation in the case of loads zero and 0.014 in for the defect type, which shows that is difficult to detect the peak's amplitude that corresponds to the BSF frequency (Fig. 17a). Meanwhile, concerning the outer defect, Fig. 17c, d shows that the peak amplitude at the BPFO is clear.

To further clarify our approach, we present another example containing three types of defects. For this example, we have chosen load one and a defect of 0.014 in. The classification results are presented in Fig. 18. These results show the number of misclassified samples in the case of the ball defect and demonstrate that the outer defect is very large. In addition, we can see that some of the samples are misclassified in the case of the outer defect. Figure 19 presents the envelope spectrum in the case of a defect of 0.014 and load one. We can observe that it is hard to detect the peak's amplitude that corresponds to the BSF and the BPFO frequencies as shown in Fig. 19a, b, e, f. This explains the lower testing accuracy.

5.2 Fault-severity Identification

Table 6 shows the classification accuracy results for each load with different bearing defect types (ball, inner, outer) for the three datasets.

(a) DE bearing (12 kHz) dataset case
The inner and outer race faults can be clearly classified using FPGA and MATLAB, with a testing accuracy of more than 92%. However, for the ball defect bearing, the testing accuracy decreased. The classification result is presented in Fig. 20 for load zero. In this worst case, a testing accuracy of 66% is obtained using FPGA.
The number of misclassified samples in the case of a 0.014 in defect is very high using both MATLAB and FPGA. Additionally, the number of misclassified samples in the case of a 0.028 in defect using FPGA is large compared to that obtained using MATLAB. To explain this decrease in precision, the representation of the envelope spectrums is presented in Fig. 21. It is difficult to detect the peak's amplitude that corresponds to the BSF frequency for the defects of 0.014 in (Fig. 21c, d). In addition, for the 0.028 in defect, the peak's amplitude of the BSF frequency using MATLAB is clear compared to the peak's amplitude using FPGA.

(b) FE bearing dataset case
These results are similar to the results that were obtained in the case of the DE bearing fault-severity identification, where the inner and outer faults can be classified easily (with a test accuracy of over 88.75%), while the MLP classifier performs worse for the ball fault. Figure 22 presents the classification results of the ball fault for load zero. As these results show, most samples are misclassified in all cases of ball defects for both implementations (FPGA and MATLAB). To understand the poor performance in this case, the envelope spectrum of the ball fault in load zero is shown in Fig. 23. It can be observed that all the peak's amplitudes in the BSF are unclear for the different cases of ball faults (0.007 in, 0.014 in, and 0.021 in). This explains the difficulty that was encountered in the classification.

(c) DE (48 kHz) dataset case

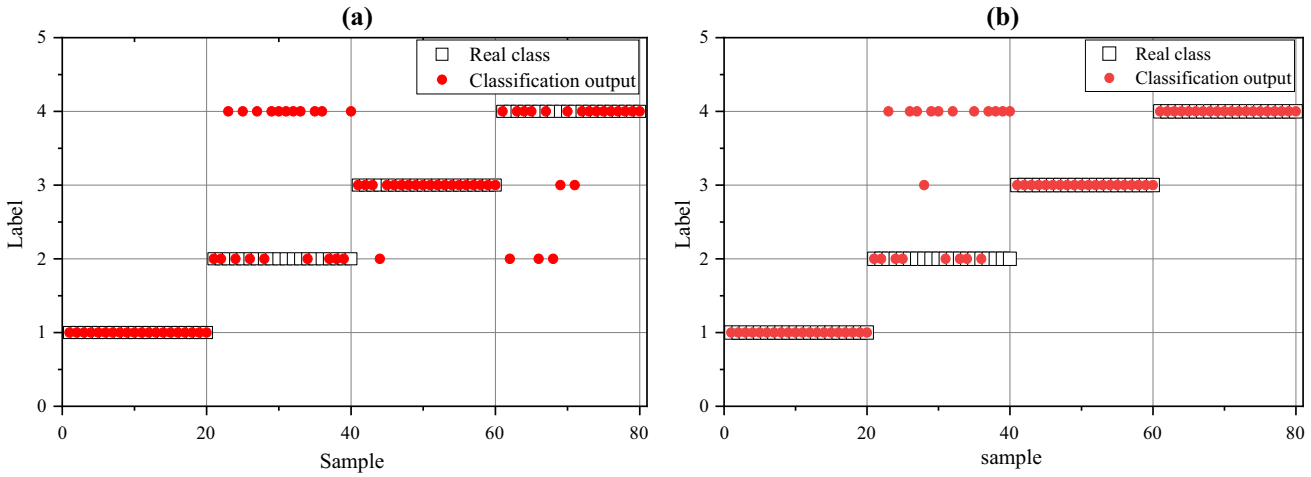


Fig. 12 Classification results in the case of DE bearing (12 kHz), 0.014 in, load 0: **a** using FPGA, **b** using MATLAB

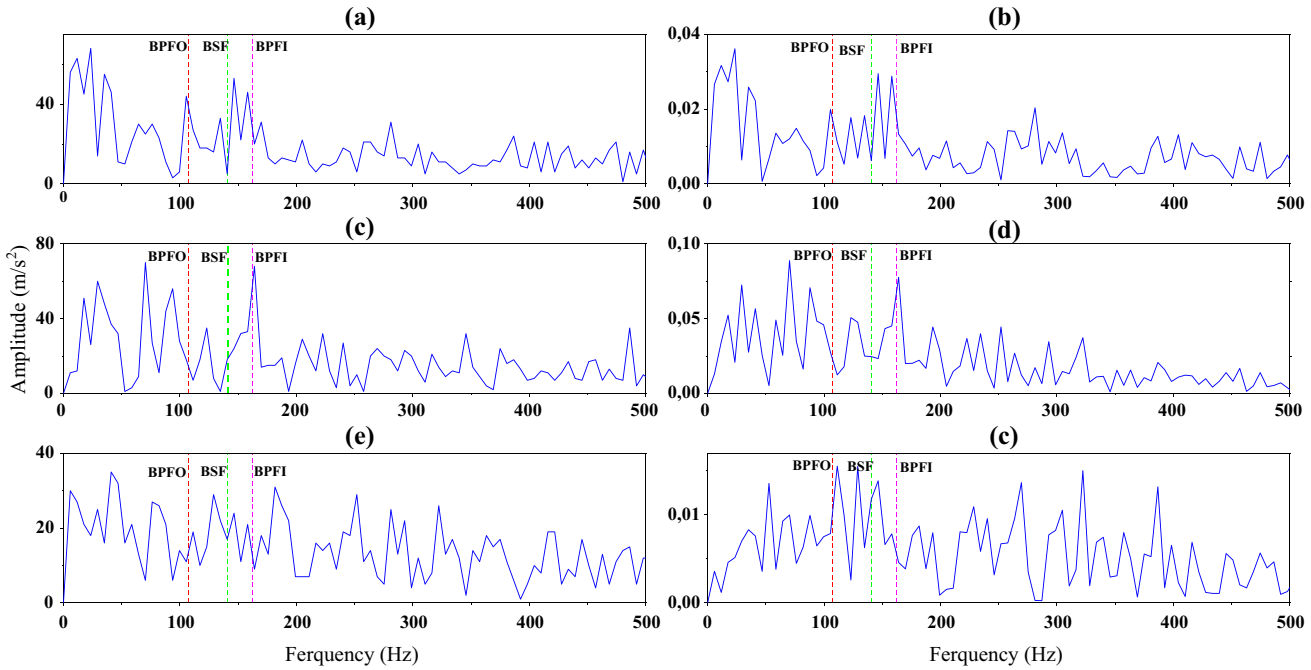


Fig. 13 Envelope spectrum (DE (12 kHz), 0.014 in, load 0): **a** ball fault (FPGA), **b** ball fault (MATLAB), **c** inner fault (FPGA), **d** inner fault (MATLAB), **e** outer fault (FPGA), **f** outer fault (MATLAB)

The results that were obtained for this experience correspond to those obtained from previous experiences, where the outer and inner defects can easily be identified, whereas the ball defect is difficult to detect. The minimum testing accuracy is achieved for load three and the ball fault. The classification results of this case are displayed in Fig. 24. Many samples are misclassified for the bearing, with defects of 0.007 in, 0.014 in and 0.021 in. Figure 25 presents the envelope spectrum of the ball fault and shows that the peak's amplitude that corresponds to the BSF frequency is unclear.

5.3 General Discussion of the Results Obtained Using the Implemented System on FPGA

In this subsection, we discuss the results that were obtained using FPGA implementation concerning the two tests that were cited in detail previously, which can easily diagnose many datasets.

First, regarding the DE (12 kHz) dataset, only two categories of the 0.014 in fault width (loads zero and three) recorded a testing accuracy of less than 90% (78.75 and 87.5, respectively). Second, concerning the FE dataset, the 0.007 in category recorded the worst testing accuracy of 70% in all

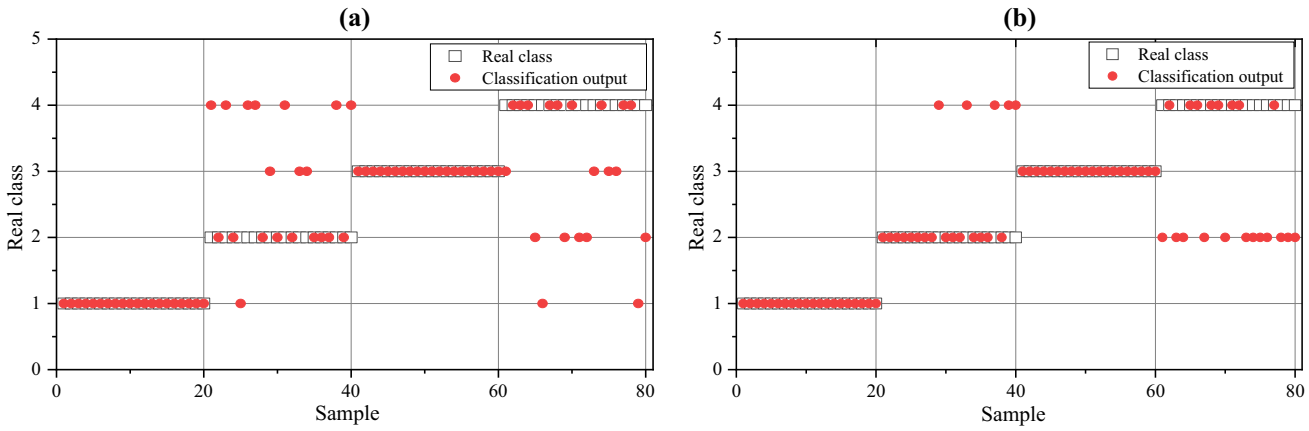


Fig. 14 Classification results in the case of FE bearing, 0.007 in: **a** using FPGA, load 2, **b** using MATLAB, load 3

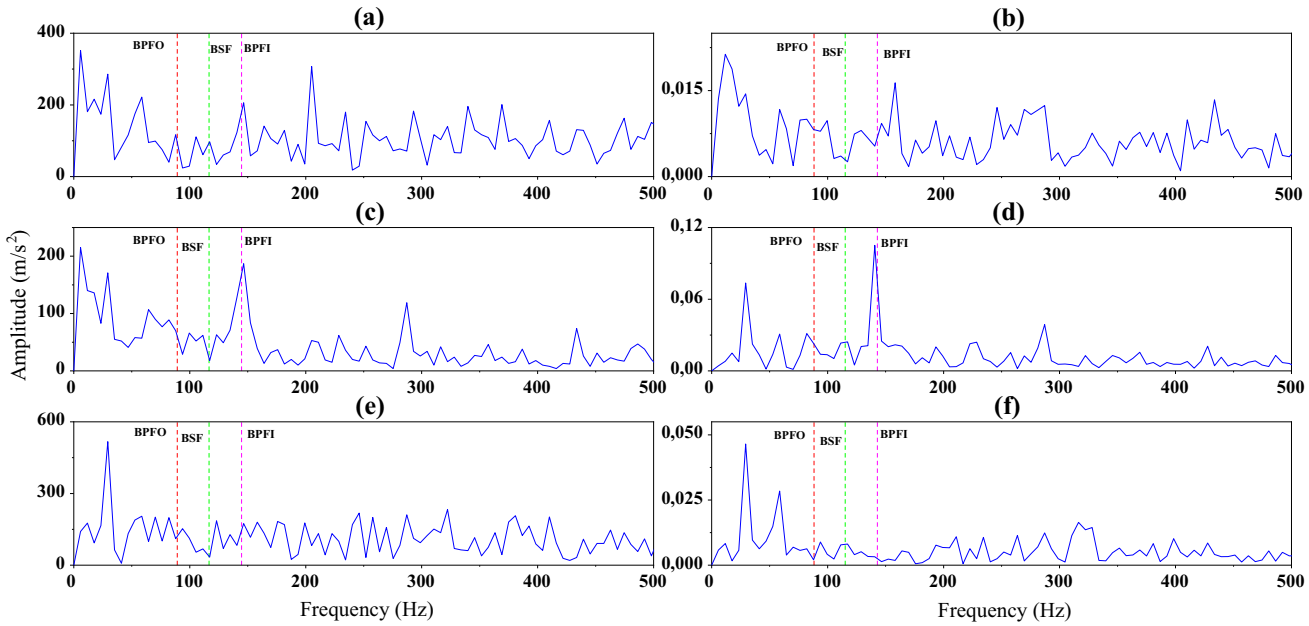


Fig. 15 Envelope spectrum (FE, 0.007 in): **a** ball fault (FPGA, load 2), **b** ball fault (MATLAB, load 3), **c** inner fault (FPGA, load 2), **d** inner fault (MATLAB, load 3), **e** outer fault (FPGA, load 2), **f** outer fault (MATLAB, load 3)

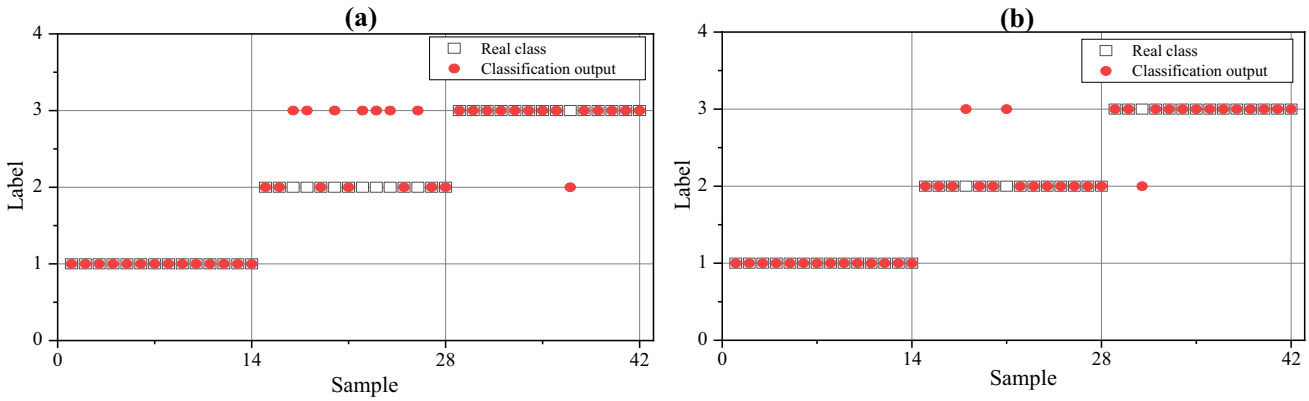


Fig. 16 Classification results in the case of DE bearing (48 kHz), 0.014 in, load 0: **a** using FPGA, **b** using MATLAB

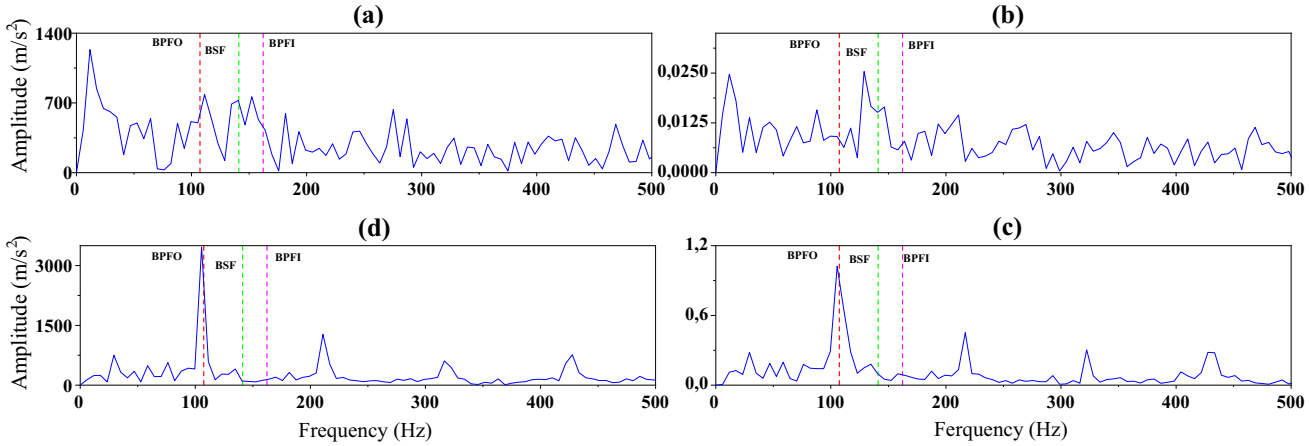


Fig. 17 Envelope spectrum (DE (48 kHz), 0.014 in, load 0): **a** ball fault (FPGA), **b** ball fault (MATLAB), **c** outer fault (FPGA), **d** outer fault (MATLAB)

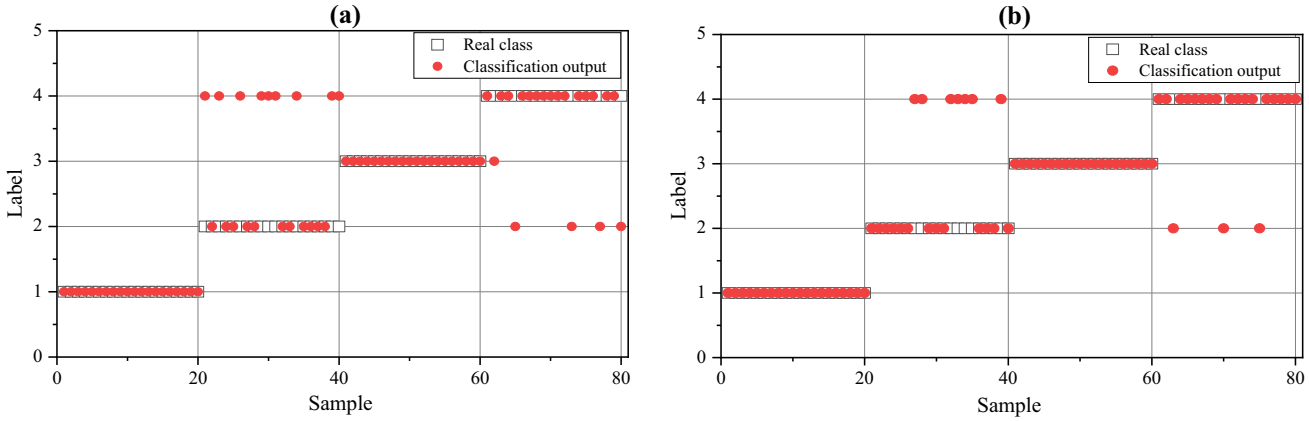


Fig. 18 Classification results in the case of DE bearing (48 kHz), 0.014 in, load 1: **a** using FPGA, **b** using MATLAB

cases. Third, the results of the DE (48 kHz) dataset were like those obtained at 12 kHz. However, a lower accuracy in the case of the 0.014 in category was recorded at 80% in most cases. Fourth, regarding the fault-severity identification of the three datasets, the inner and outer fault types were easily detected. Nevertheless, it is difficult to identify the ball fault.

In addition, the results of the implementation on FPGA show that they are lower than those obtained with MATLAB simulations due to using fixed-point computations during the features parameters extraction phase to minimise the consumption of physical resources on the FPGA circuit. This results in less energy consumption and faster computing.

5.4 Comparison with Previous Work

In this subsection, we compare our results with others that use the CWRU database in the same way as presented above and the same testing scenarios. In this context, the recent study in [28] adopted similar benchmark methodology. The comparison is limited to the BPNN-type classifier, which is similar to ours. In addition, it should be noted that their study is limited to simulations, whereas ours targets a physical implementation of FPGA.

Tables 7 and 8 show that the simulation results using MATLAB of the proposed method provide an average accuracy approximately 98.4 and 94% for fault-type and fault-severity identifications, respectively, which are better than those mentioned in [28]. In Figure 26a, the boxplots show that 75% of our results have an accuracy greater than 99.4%, while 75% for the TFF method have an accuracy greater than 93% for the fault-type identification. In addition, regarding the fault-severity, Fig. 26b shows the superiority of our proposed method. Therefore, 75% of the results have an accuracy greater than 91%, while 75% for the MPE method have an accuracy greater than 90%.

Our results using FPGA provide an average accuracy of 94.84% for fault-type identification and 88.81% for fault-severity identification. The boxplots in Fig. 26 show that 75% of the results provide an accuracy of over 92.3% for

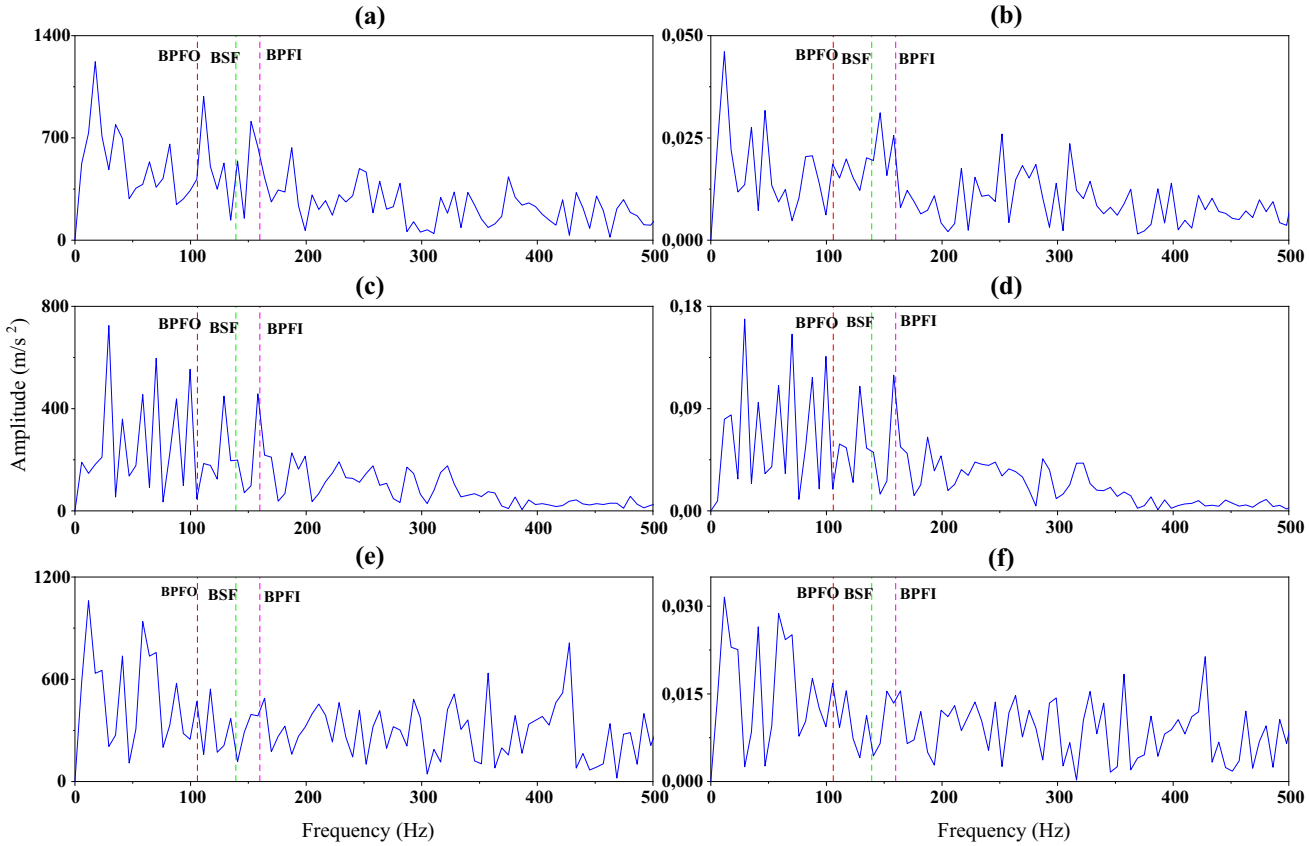


Fig. 19 Envelope spectrum (DE (48 kHz), 0.014 in, load 1). **a** ball fault (FPGA), **b** ball fault (MATLAB), **c** inner fault (FPGA), **d** inner fault (MATLAB), **e** outer fault (FPGA), **d** outer fault (MATLAB)

Table 6 Result of classification accuracy of fault-severity identification

Fault width (in)	Load (hp)	DE (12 kHz) dataset		FE (12 kHz) dataset		DE (48 kHz) dataset	
Fault type		Using MATLAB	Using FPGA	Using MATLAB	Using FPGA	Using MATLAB	Using FPGA
Ball	0	83	66	70	61.25	89.25	85.71
	1	86	67	76.25	78.75	77.5	67.5
	2	91	75	86.25	76.25	78.75	68.75
	3	91	68	93.75	87.5	73.75	53.75
	Mean	**87.5**	**69**	**81.56**	**75.93**	**79.82**	**68.92**
Inner race	0	92	98	92.5	91.25	90.48	92.86
	1	95	99	100	95	100	100
	2	99	99	100	98.75	100	100
	3	93	95	100	95	82.5	83.75
	Mean	**94.75**	**97.75**	**98.12**	**95**	**93.24**	**94.15**
Outer race	0	100	100	100	95	100	98.21
	1	100	100	95	98.75	100	98.75
	2	100	100	98.75	88.75	100	98.75
	3	100	98.75	98.75	95	100	95
	Mean	**100**	**99.69**	**98.12**	**94.37**	**100**	**97.68**

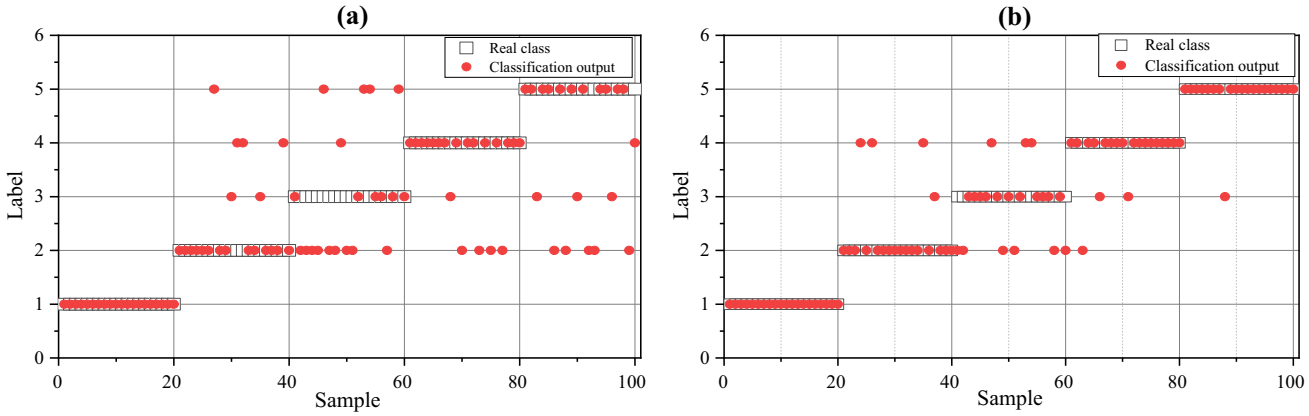


Fig. 20 Classification results in the case of DE ball fault (12 kHz), load 0: **a** using FPGA, **b** using MATLAB

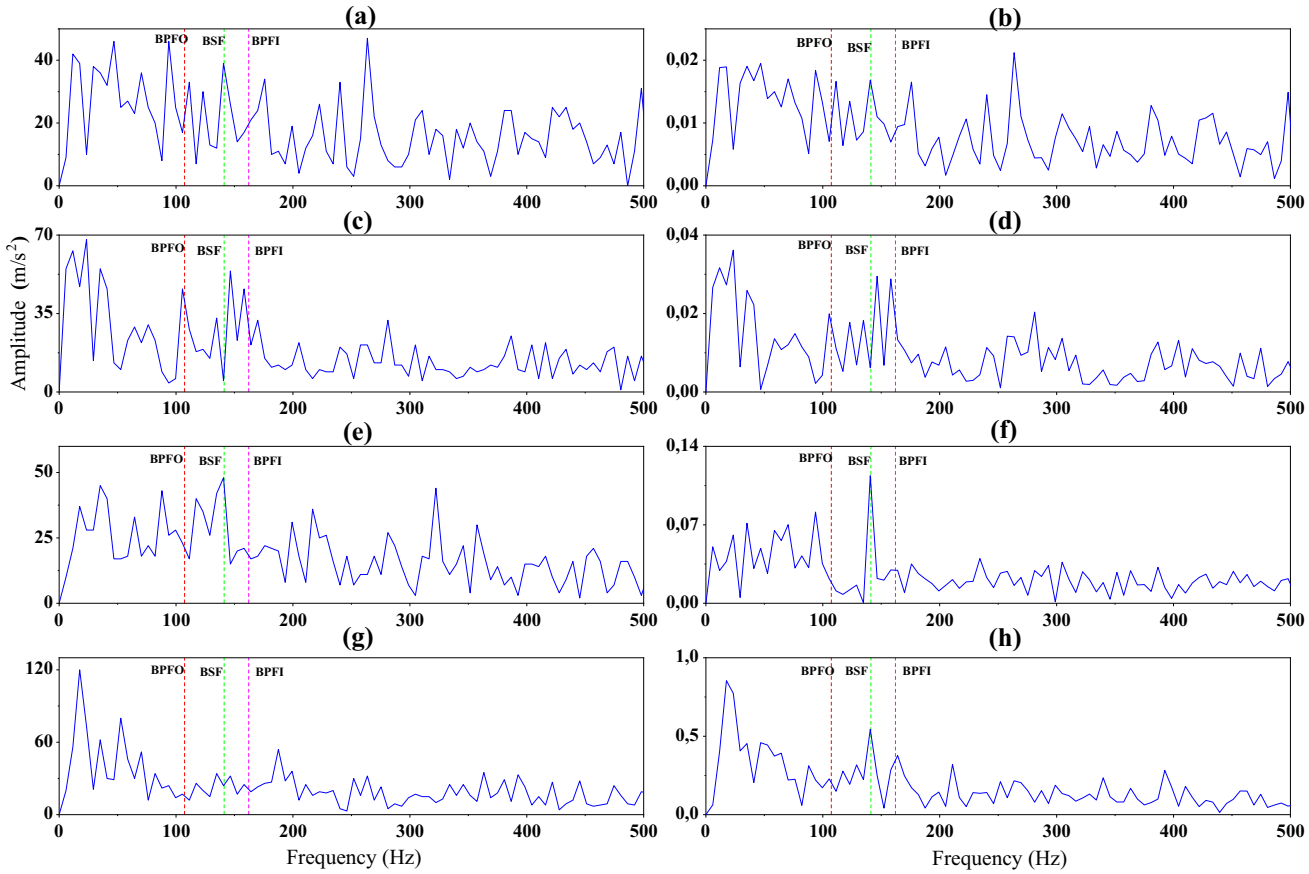


Fig. 21 Envelope spectrum (DE (12 kHz), ball fault, load 0): **a** 0.007 in fault (FPGA), **b** 0.007 in fault (MATLAB), **c** 0.014 in fault (FPGA), **d** 0.014 in fault (MATLAB), **e** 0.021 in fault (FPGA), **f** 0.021 in fault (MATLAB), **g** 0.028 in fault (FPGA), **h** 0.028 in fault (MATLAB)

the fault-type identification and 71.5% for the fault-severity identification.

5.5 Processing Time Results

In this subsection, the results of the processing time measurements are presented for the two implementations (MATLAB on PC and the FPGA). Regarding the first implementation, the MATLAB 2018a software is run on a laptop with a 2.6 GHz i5-7300U processor and 8 GB of random-access memory (RAM). Regarding the second implementation, a timer is added to measure the processing time. The results that are presented in Table 9 show that in the case of the FPGA, the maximum time that is required to complete the

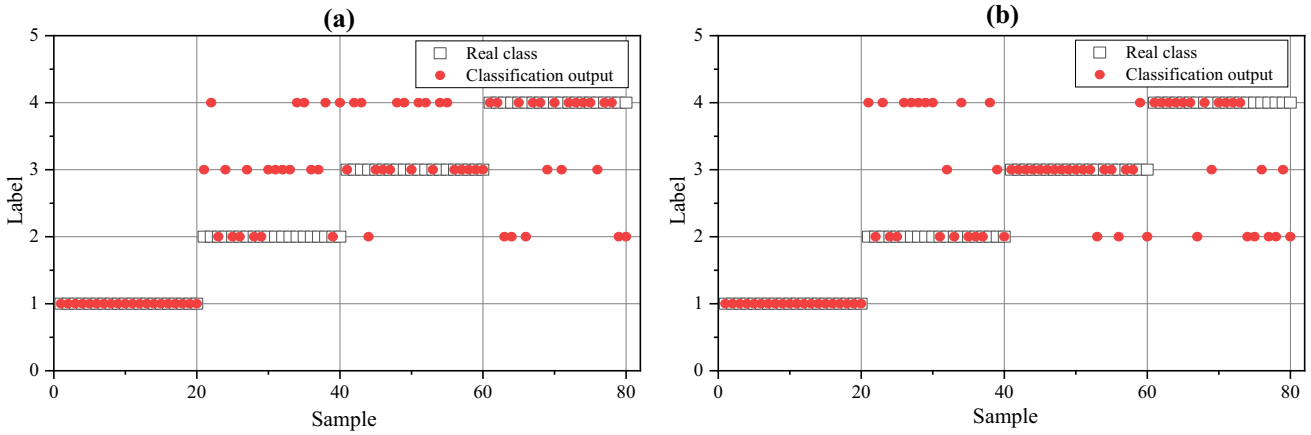


Fig. 22 Classification results in the case of FE ball fault, load 0: **a** using FPGA, **b** using MATLAB

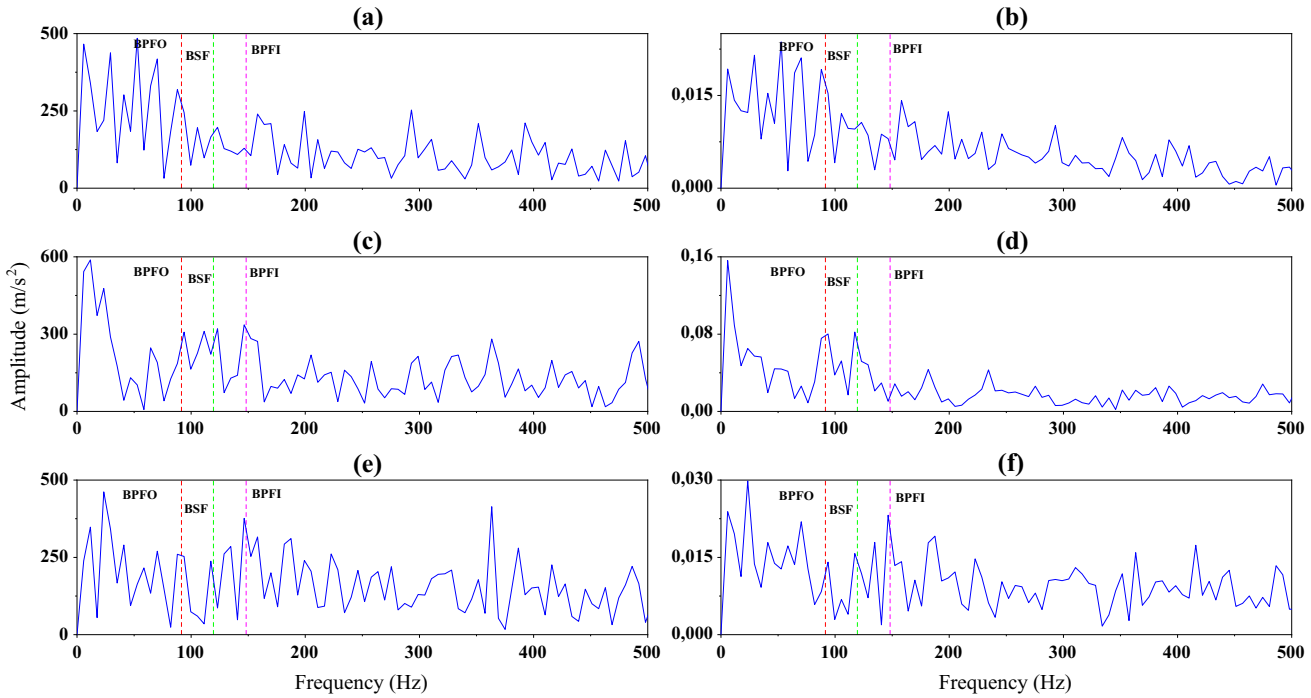


Fig. 23 Envelope spectrum (FE, ball fault, load 0): **a** 0.007 in fault (FPGA), **b** 0.007 in fault (MATLAB), **c** 0.014 in fault (FPGA), **d** 0.014 in fault (MATLAB), **e** 0.021 in fault (FPGA), **f** 0.021 in fault (MATLAB)

processing of all samples is less than 1.6 s, which remains promising for embedded systems, and approximately 259 ms for the MATLAB implementation.

6 Conclusion

In this research, an embedded intelligent system has been designed to identify the bearing fault types (ball, inner race and outer race faults) and the degree of severity.

Our first contribution was to propose a system that used the envelope analysis to process the raw vibration signals that are obtained from the CWRU dataset to obtain the amplitudes of peaks that correspond to the bearing fault frequencies that are used as inputs for the MLP network classifier. The obtained results that were simulated by MATLAB show that it is possible to achieve an average accuracy of approximately 98.4 and 94% for the fault-type and fault-severity identifications, respectively, for the DE (12 kHz) dataset, which provides

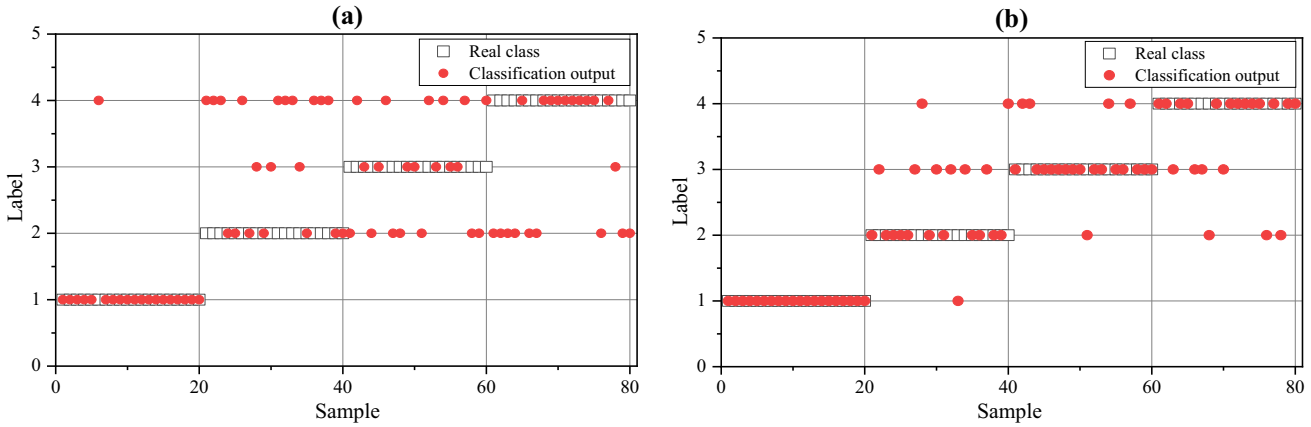


Fig. 24 Classification results in the case of DE bearing ball fault (48 kHz), load 3: **a** using FPGA, **b** using MATLAB

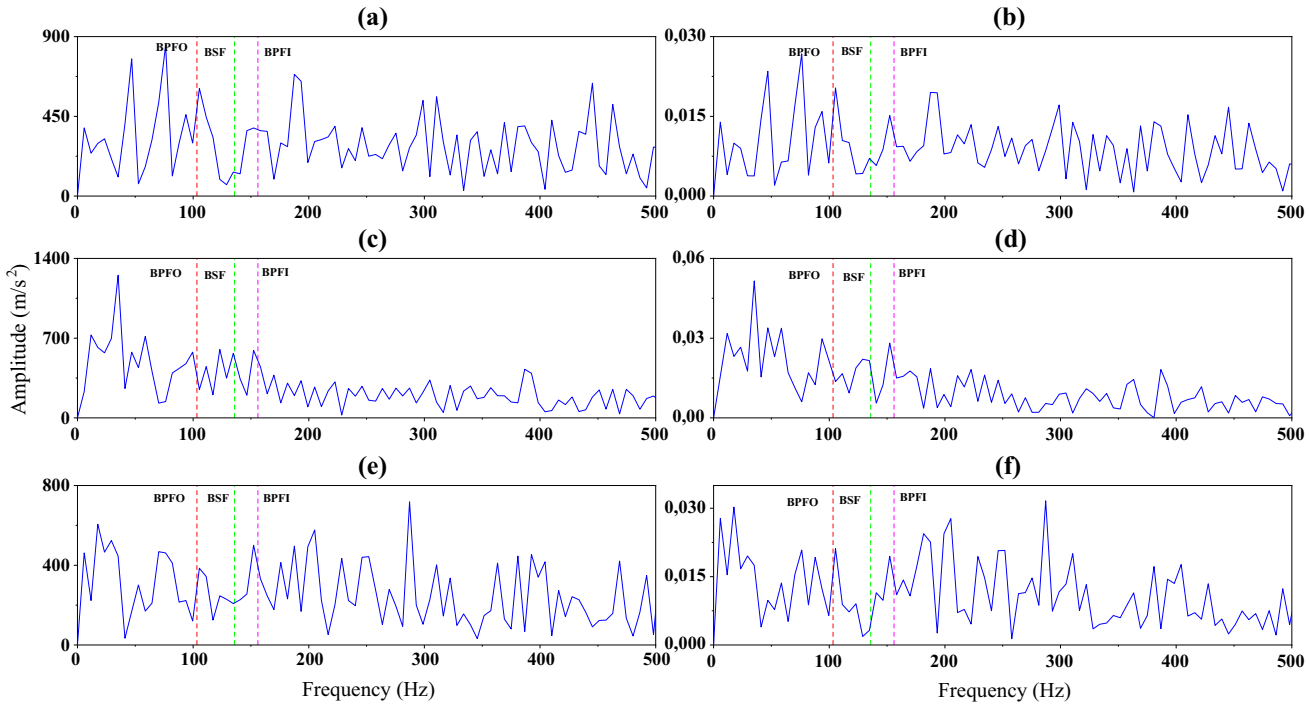


Fig. 25 Envelope spectrum (DE (48 kHz), ball fault, load 3). **a** 0.007 in fault (FPGA), **b** 0.007 in fault (MATLAB), **c** 0.014 in fault (FPGA), **d** 0.014 in fault (MATLAB), **e** 0.021 in fault (FPGA), **f** 0.021 in fault (MATLAB)

better accuracy rate compared to other similar works in the literature.

The second contribution of this work is the implementation of our diagnosis system on a low-cost and low-energy consumption FPGA circuit using a co-design approach, where different blocs are added as personalised IP-cores (FFT bloc, MLP), and a C language code executed by the ARM processor, which manages the different tasks inside the embedded system. The MLP network classifier is designed using the XSG software tool and integrated into the architecture as a co-processor, where the different parameters of the network had already been obtained from offline training.

The obtained practical results provide an average accuracy of 95 and 89% for the fault-type and the fault-severity identifications, respectively, for the DE (12 kHz) dataset. In addition, the results show that the implementation consumes approximately 65% of LUTs resources. Therefore, future studies could use the rest of the resources to add a communication module to realise a wireless sensor node. Several nodes can form an industrial wireless sensor network (IWSN) as a diagnostic system, which constitutes the main part of the industrial internet of things (IIoT). Further work could combine the bearing faults with other mechanical and electrical faults.

Table 7 Comparison results of classification accuracy test of fault-type identification using DE (12 kHz) bearing data

Fault width (in)	Load (hp)	Proposed method using MATLAB	Proposed method using FPGA	BPNN [28] (MFE method)	BPNN [28] (MSE method)	BPNN [28] (MPE method)	BPNN [28] (TFF method)
0.007	0	100	100	91.25	92.5	95	100
	1	100	100	95	81.25	96.25	100
	2	100	100	98.75	92.5	95	100
	3	100	98.75	92.5	88.75	97.5	100
	Mean	**100**	**99.69**	**94.38**	**88.75**	**95.94**	**100**
0.014	0	85	78.75	85	73.75	88.75	73.75
	1	98.75	93.75	87.5	76.25	90	87.5
	2	95	91.25	98.75	75	92.5	80
	3	96.25	87.5	91.25	80	88.75	76.25
	Mean	**93.75**	**87.81**	**90.63**	**76.25**	**90**	**79.38**
0.021	0	100	96.25	91.25	90	100	98.75
	1	100	100	97.5	87.5	91.25	98.75
	2	100	100	95	81.25	96.25	100
	3	100	91.25	96.25	92.5	100	98.75
	Mean	**100**	**96.87**	**95**	**87.81**	**96.88**	**99.06**
0.028	0	100	95	100	98.33	100	100
	1	100	95	100	98.33	100	100
	2	100	93.33	100	98.33	96.67	98.33
	3	100	96.67	100	100	100	100
	Mean	**100**	**95**	**100**	**98.75**	**99.17**	**99.58**
	Total mean	**98.44**	**94.84**	**95**	**87.89**	**95.5**	**94.5**

Table 8 Comparison results of classification accuracy test of fault-severity identification using DE (12 kHz) bearing data

Fault type	Load (hp)	Proposed method using MATLAB	Proposed method using FPGA	BPNN [28] (MFE method)	BPNN [28] (MSE method)	BPNN [28] (MPE method)	BPNN [28] (TFF method)
Ball	0	83	66	54	61	70	54
	1	86	67	76	61	91	61
	2	91	75	62	71	90	84
	3	91	68	89	64	93	58
	Mean	**87.5**	**69**	**70.25**	**64.25**	**86**	**64.25**
Inner race	0	92	98	87	72	87	99
	1	95	99	90	51	92	89
	2	99	99	87	80	99	81
	3	93	95	72	74	100	88
	Mean	**94.75**	**97.75**	**84**	**69.25**	**94.5**	**89.25**
Outer race	0	100	100	97.5	72.5	92.5	98.75
	1	100	100	97.5	96.25	100	100
	2	100	100	93.75	83.75	96.25	98.75
	3	100	98.75	95	91.25	95	100
	Mean	**100**	**99.69**	**95.94**	**85.94**	**95.94**	**99.38**
	Total mean	**94.08**	**88.81**	**83.4**	**73.14**	**92.15**	**84.29**

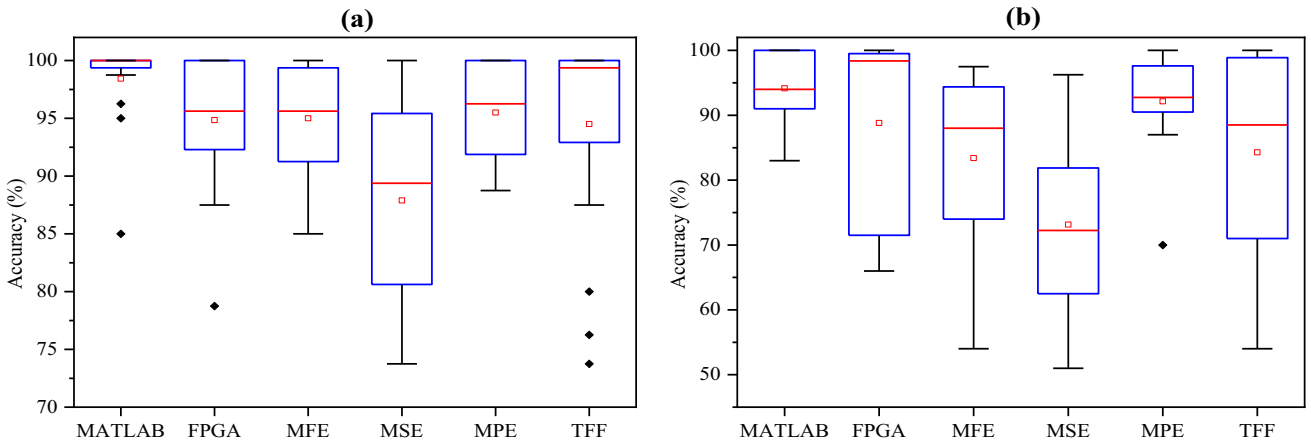


Fig. 26 Boxplots of the obtained results, **a** case of fault-type identification, **b** case of fault-severity identification

Table 9 Maximum time processing required (ms)

	2048 points		8192 points	
	Using FPGA	Using MATLAB	Using FPGA	Using MATLAB
Envelope spectrum	3.122	1.654	14.484	5.614
MLP processing	13.439	9.965	13.439	9.691
Entire sample processing	16.499	11.456	27.902	14.923
All data samples	972.290	220.517	1593.795	259.076

Acknowledgements This research work is fully supported by the Directorate General for Scientific Research and Technological Development (DGRSDT), Algeria. The software is provided by Xilinx under Xilinx University Program (XUP).

References

1. Attoui, I.; Oudjani, B.; Boutasseta, N.; Fergani, N.; Bouakkaz, M.; Bouraiou, A.: Novel predictive features using a wrapper model for rolling bearing fault diagnosis based on vibration signal analysis. Int. J. Adv. Manuf. Technol. **106**, 3409–3435 (2020). https://doi.org/10.1007/s00170-019-04729-4
2. Zhang, Y.; Ren, G.; Wu, D.; Wang, H.: Rolling bearing fault diagnosis utilizing variational mode decomposition based fractal dimension estimation method. Measurement **181**, 109614 (2021). https://doi.org/10.1016/j.measurement.2021.109614
3. Duan, Z.; Wu, T.; Guo, S.; Shao, T.; Malekian, R.; Zhixiong, L.: Development and trend of condition monitoring and fault diagnosis of multi-sensors information fusion for rolling bearings : a review. Int. J. Adv. Manuf. Technol. **96**, 803–819 (2018). https://doi.org/10.1007/s00170-017-1474-8
4. Tingarikar, G.; Choudhury, A.: Vibration analysis—based fault diagnosis of a dynamically loaded bearing with distributed defect. Arab. J. Sci. Eng. (2021). https://doi.org/10.1007/s13369-021-05862-7
5. Niu, X.; Zhu, L.; Ding, H.: New statistical moments for the detection of defects in rolling element bearings. Int. J. Adv. Manuf. Technol. **26**, 1268–1274 (2005). https://doi.org/10.1007/s00170-004-2109-4
6. Siegel, D.; Ly, C.; Lee, J.: Methodology and framework for predicting helicopter rolling element bearing failure. IEEE Trans. Reliab. **61**, 846–857 (2012). https://doi.org/10.1109/ICPHM.2011.6024339
7. Gligorijevic, J.; Gajic, D.; Brkovic, A.; Savic-Gajic, I.; Georgieva, O.; Di Gennaro, S.: Online condition monitoring of bearings to support total productive maintenance in the packaging materials industry. Sensors **16**, 1–16 (2016). https://doi.org/10.3390/s16030316
8. Lin, H.; Ye, Y.-C.: Reviews of bearing vibration measurement using fast Fourier transform and enhanced fast Fourier transform algorithms. Adv. Mech. Eng. **11**, 1–12 (2019). https://doi.org/10.1177/1687814018816751
9. Feng, G.J.; Gu, J.; Zhen, D.; Aliwan, M.; Gu, F.S.; Ball, A.D.: Implementation of envelope analysis on a wireless condition monitoring system for bearing fault diagnosis. Int. J. Autom. Comput. **12**, 14–24 (2015). https://doi.org/10.1007/s11633-014-0862-x
10. Ibarra-zarate, D.; Tamayo-pazos, O.; Vallejo-guevara, A.: Bearing fault diagnosis in rotating machinery based on cepstrum prewhitening of vibration and acoustic emission. Int. J. Adv. Manuf. Technol. **104**, 4155–4168 (2019). https://doi.org/10.1007/s00170-019-04171-6
11. Park, C.; Choi, Y.; Kim, Y.H.: Early fault detection in automotive ball bearings using the minimum variance cepstrum. Mech. Syst. Signal Process. **38**, 534–548 (2013). https://doi.org/10.1016/j.ymssp.2013.02.017
12. Lee, D.; Hong, C.; Jeong, W.; Ahn, S.: Applied sciences time—frequency envelope analysis for fault detection of rotating machinery signals with impulsive noise. Appl. Sci. **11**, 1–16 (2021). https://doi.org/10.3390/app11125373

13. Fei, S.: Fault diagnosis of bearing based on wavelet packet transform-phase space reconstruction-singular value decomposition and SVM classifier. Arab. J. Sci. Eng. **42**, 1967–1975 (2017). https://doi.org/10.1007/s13369-016-2406-x
14. Wang, C.; Gan, M.; Zhu, C.: Fault feature extraction of rolling element bearings based on wavelet packet transform and sparse representation theory. J. Intell. Manuf. **29**, 937–951 (2018). https://doi.org/10.1007/s10845-015-1153-2
15. Zhang, J.; Huang, D.; Yang, J.; Liu, H.; Liu, X.: Realizing the empirical mode decomposition by the adaptive stochastic resonance in a new periodical model and its application in bearing fault diagnosis. J. Mech. Sci. Technol. **31**, 4599–4610 (2017). https://doi.org/10.1007/s12206-017-0906-6
16. Wang, J.; Du, G.; Zhu, Z.; Shen, C.; He, Q.: Fault diagnosis of rotating machines based on the EMD manifold. Mech. Syst. Signal Process. **135**, 1–21 (2020). https://doi.org/10.1016/j.ymssp.2019.106443
17. Boudiaf, A.; Moussaoui, A.; Dahane, A.; Atoui, I.: A comparative study of various methods of bearing faults diagnosis using the Case Western Reserve University Data. J. Fail. Anal. Prev. **16**, 271–284 (2016). https://doi.org/10.1007/s11668-016-0080-7
18. Bokde, N.; Feijóo, A.; Villanueva, D.; Kulat, K.: A review on hybrid empirical mode decomposition models for wind speed and wind power prediction. Energies **12**, 1–42 (2019). https://doi.org/10.3390/en12020254
19. Liu, C.; Cichon, A.; Królczyk, G.; Li, Z.: Technology development and commercial applications of industrial fault diagnosis system: a review. Int. J. Adv. Manuf. Technol. (2021). https://doi.org/10.1007/s00170-021-08047-6
20. Guo, L.; Chen, J.; Li, X.: Rolling bearing fault classification based on envelope spectrum and support vector machine. J. Vib. Control **15**, 1349–1363 (2009). https://doi.org/10.1177/1077546308095224
21. Tyagi, S.; Panigrahi, S.K.: An improved envelope detection method using particle swarm optimisation for rolling element bearing fault diagnosis. J. Comput. Des. Eng. **4**, 305–317 (2017). https://doi.org/10.1016/j.jcde.2017.05.002
22. Amini, A.; Entezami, M.; Papaelias, M.: Onboard detection of railway axle bearing defects using envelope analysis of high frequency acoustic emission signals. Case Stud. Nondestruct. Test. Eval. **6**, 8–16 (2016). https://doi.org/10.1016/j.csndt.2016.06.002
23. Smith, W.A.; Randall, R.B.: Rolling element bearing diagnostics using the Case Western Reserve University data: a benchmark study. Mech. Syst. Signal Process. **64–65**, 100–131 (2015). https://doi.org/10.1016/j.ymssp.2015.04.021
24. Liu, R.; Yang, B.; Zio, E.; Chen, X.: Artificial intelligence for fault diagnosis of rotating machinery: a review. Mech. Syst. Signal Process. **108**, 33–47 (2018). https://doi.org/10.1016/j.ymssp.2018.02.016
25. Unal, M.; Onat, M.; Demetgul, M.; Kucuk, H.: Fault diagnosis of rolling bearings using a genetic algorithm optimized neural network. Measurement **58**, 187–196 (2014). https://doi.org/10.1016/j.measurement.2014.08.041
26. Ben Ali, J.; Fnaiech, N.; Saidi, L.; Chebel-morello, B.; Fnaiech, F.: Application of empirical mode decomposition and artificial neural network for automatic bearing fault diagnosis based on vibration signals. Appl. Acoust. **89**, 16–27 (2015). https://doi.org/10.1016/j.apacoust.2014.08.016
27. Kuncan, M.; Kaplan, K.; Recep, M.; Kaya, Y.; Ertunç, H.M.: A novel feature extraction method for bearing fault classification with one dimensional ternary patterns. ISA Trans. J. **100**, 346–357 (2020). https://doi.org/10.1016/j.isatra.2019.11.006
28. Li, Y.; Wang, X.; Si, S.; Huang, S.: Entropy based fault classification using the Case Western Reserve University data: a benchmark study. IEEE Trans. Reliab. **69**, 754–767 (2020). https://doi.org/10.1109/TR.2019.2896240
29. Welcome to the Case Western Reserve University Bearing Data Center Website | Bearing Data Center (n.d.). https://csegroups.case.edu/bearingdatacenter/pages/welcome-case-western-reserve-university-bearing-data-center-website. Accessed 22 Mar 2020
30. Laala, W.; Guedidi, A.; Guettaf, A.: Bearing faults classification based on wavelet transform and artificial neural network. Int. J. Syst. Assur. Eng. Manag. (2020). https://doi.org/10.1007/s13198-020-01039-x
31. Sikder, N.; Shamim, A.; Arif, M.; Islam, M.M.M.; Al, A.: Induction motor bearing fault classification using extreme learning machine based on power features. Arab. J. Sci. Eng. **46**, 8475–8491 (2021). https://doi.org/10.1007/s13369-021-05527-5
32. Bicakci, S.; Coramik, M.; Gunes, H.; Citak, H.; Ege, Y.: A new artificial neural network—based failure determination system for electric motors. Arab. J. Sci. Eng. (2021). https://doi.org/10.1007/s13369-021-05594-8
33. Meserkhani, A.; Jafari, S.M.; Rahi, A.: Experimental comparison of acoustic emission sensors in the detection of outer race defect of angular contact ball bearings by artificial neural network. Measurement **168**, 108198 (2021). https://doi.org/10.1016/j.measurement.2020.108198
34. Seng, K.P.; Lee, P.J.; Ang, L.M.: Embedded intelligence on FPGA: survey, applications and challenges. Electronics **10**, 1–33 (2021). https://doi.org/10.3390/electronics10080895
35. Ghazi Blaiech, A.; Ben Khalifa, K.; Valderrama, C.; Fernandes, M.A.C.; Hedi Bedoui, M.: A survey and taxonomy of FPGA-based deep learning accelerators. J. Syst. Archit. **98**, 331–345 (2019). https://doi.org/10.1016/j.sysarc.2019.01.007
36. Saidi, A.; Ben Othman, S.; Dhouibi, M.; Ben Saoud, S.: FPGA-based implementation of classification techniques: a survey. Integration **81**, 280–299 (2021). https://doi.org/10.1016/j.vlsi.2021.08.004
37. Kang, M.; Kim, J.; Kim, J.M.: An FPGA-based multicore system for real-time bearing fault diagnosis using ultrasampling rate AE signals. IEEE Trans. Ind. Electron. **62**, 2319–2329 (2015). https://doi.org/10.1109/TIE.2014.2361317
38. Camarena-Martinez, D.; Valtierra-Rodriguez, M.; Garcia-Perez, A.; Osornio-Rios, R.A.; Romero-Troncoso, R.D.J.: Empirical mode decomposition and neural networks on FPGA for fault diagnosis in induction motors. Sci. World J. **2014**, 1–17 (2014). https://doi.org/10.1155/2014/908140
39. Contreras-hernandez, J.L.; Almanza-ojeda, D.L.; Ledesma, S.; Ibarra-manzano, M.A.: Motor fault detection using Quaternion Signal Analysis on FPGA. Measurement **138**, 416–424 (2019). https://doi.org/10.1016/j.measurement.2019.01.088
40. Cabal-yepez, E.; Valtierra-rodriguez, M.; Romero-troncoso, R.J.; Garcia-perez, A.; Osornio-Rios, R.A.; Miranda-Vidales, H.; Alvarez-Salas, R.: FPGA-based entropy neural processor for online detection of multiple combined faults on induction motors. Mech. Syst. Signal Process. **30**, 123–130 (2012). https://doi.org/10.1016/j.ymssp.2012.01.021
41. Bengherbia, B.; Ould Zmirli, M.; Toubal, A.; Guessoum, A.: FPGA-based wireless sensor nodes for vibration monitoring system and fault diagnosis. Measurement **101**, 81–92 (2017). https://doi.org/10.1016/j.measurement.2017.01.022
42. Bengherbia, B.; Kara, R.; Toubal, A.; Ould Zmirli, M.; Chadli, S.; Wira, P.: FPGA implementation of a wireless sensor node with a built-in ADALINE neural network coprocessor for vibration analysis and fault diagnosis in machine condition monitoring. Measurement **163**, 107960 (2020). https://doi.org/10.1016/j.measurement.2020.107960
43. McInerny, S.A.; Dai, Y.: Basic vibration signal processing for bearing fault detection. IEEE Trans. Educ. **46**, 149–156 (2003). https://doi.org/10.1109/TE.2002.808234

44. Acoustics, O.N.: FFT pruning applied to time domain interpolation and peak localization. IEEE Trans. Acoust. **35**, 1776–1778 (1987). https://doi.org/10.1109/TASSP.1987.1165102

45. Marple, S.L.: Computing the discrete-time "Analytic" signal via FFT. IEEE Trans. SIGNAL Process. **47**, 2600–2603 (1999). https://doi.org/10.1109/78.782222